A concurrent multiscale method based on the meshfree method and molecular dynamics analysis

Y. T. Gu and L. C. Zhang*

School of Aerospace, Mechanical & Mechatronic Engineering,
University of Sydney, NSW, 2006, Australia

Abstract

This paper presents a concurrent simulation technique for analysing the deformation of systems that need the integration of material properties from nanoscopic to macroscopic dimensional scales. In the continuum sub-domain, a weak-form based meshfree method using the radial basis function interpolation was employed, but in the atomic sub-domain, molecular dynamics analysis was used. The transition from the atomic to continuum domains was realized by transition particles which are independent of either the nodes in the continuum sub-domain or the atoms in the atomic sub-domain. A simple penalty method was used to ensure the compatibility of displacements and their gradients in the transition. A virtual cell algorithm was developed using a local quasi-continuum approach to obtain the equivalent continuum strain energy density based on the atomic potentials and Cauchy-Born rule. Numerical examples showed that the present method is very accurate and stable, and has a promising potential to a wide class of multiscale systems.

Keywords: Multiscale analysis; Meshfree method; Molecular dynamics; Coupling; Continuum; Atomic

* Corresponding author. E-mail: zhang@aeromech.usyd.edu.au

Nomenclature

Φ	shape function, defined in Eq. (22)
$\dot{u}$,$\ddot{u}$	First and second derivatives of u with respect to time, respectively
b_i	body force, defined in Eq. (7)
a, **b**	vector of interpolation coefficients, defined in Eq. (10)
$\mathbf{B}_m$, $\mathbf{R}_0$, $\mathbf{G}$	Interpolation matrices in the radial basis function (RBF) interpolation, defined in Eqs. (13) and (17)
c_0	dimensionless coefficient in multi-quadric RBF, defined in Eq. (11)
d_i	nodal spacing in multi-quadric RBF, defined in Eq. (11)
F	deformation gradient, defined in Eq. (9)
$\mathbf{f}_k^{\mathrm{c}}$, $\mathbf{f}_k^{\mathrm{a}}$	forces at a transition particle k computed in continuum and atomic domains, defined in Eq. (41)
$\mathbf{f}_{i(c)}^{\mathrm{ext}}$, $\mathbf{f}_{i(c)}^{\mathrm{int}}$	external and internal forces for node I in the continuum domain, defined in Eq. (38)
$\mathbf{f}_{i(a)}^{\mathrm{ext}}$, $\mathbf{f}_{i(a)}^{\mathrm{int}}$	external and internal forces for atom i in the atomic domain, defined in Eq. (6)
H^c, H^a	Hamiltonian for the continuum and the atomic domains, respectively, defined in Eqs. (32) and (1)
k	spring stiffness in the harmonic potential, defined in Eq. (66)
m^c, m^a	lumped mass of the continuum node and that of an atom, respectively, defined in Eqs. (33) and (1)
N	an integer used in the multiple-time-step, defined in Eq. (61)
p_j	monomial of polynomial basis functions, defined in Eq. (10)
P_{ij}	the first Piola-Kirchhoff stress tensor, defined in Eq. (7)
q	coefficient in multi-quadric RBF, defined in Eq. (11)
r_{ij}, R_{ij}	distance between two points, defined in Eqs. (26) and (27)
R_i	radial function, defined in Eq. (10)
$\mathbf{u}^{\mathrm{c}}$, $\mathbf{u}^{\mathrm{a}}$	displacements of a transition particle obtained by the interpolations using continuum nodes and atoms, defined in Eq. (40)
T	Time
u	displacement vector, defined in Eq. (23)
v	velocity vector, defined in Eq. (24)
w^{c}	the potential energy per unit volume of the continuum, defined in Eq. (30)
w^{a}	atomic potential, defined in Eq. (30)

$\mathbf{X}$, $\mathbf{x}$	coordinate vectors in undeformed and deformed configuration
α	scaling parameter, defined in Eq. (44)
$\beta_l^{(1)}, \beta_l^{(2)}, \beta_l^{(3)}$	penalty coefficients for the transition particle l, , defined in Eqs. (46),(47), (57) and (58)
Γ	global boundary
ε, σ	Coefficient for L-J potential, defined in Eq. (68)
V^c	the volume of a considered continuum domain , defined in Eq. (30)
ρ_0	mass density, defined in Eq. (7)
$\Delta T^c, \Delta t^a$	time step for the continuum domain and the atomic domain, defined in Eq. (61)
Ω	problem domain
Ω^c , Ω^a, Ω^t	continuum domain, atomic domain, and transition domain
$\boldsymbol{\varphi}$	mapping function, defined in Eq. (8)
ζ_k	shift vector for the lattice, defined in Eq. (28)

1 Introduction

Multiscale manufacturing and characterization has been a recent focus in the development of advanced technology, and has posed new challenges, because the length scales to be analysed vary from macroscopic to nanoscopic dimensions but many analytical tools are only applicable to a single dimensional scale. For example, a common approach for nano-scale simulation is to use molecular dynamics (MD). However, an MD simulation requires the computation of a large number of atoms, which significantly limits its applicability to large systems. On the other hand, techniques like the finite element method (FEM), the finite difference method (FDM) and the finite volume method (FVM) are based on continuum mechanics theories, which become invalid for nano-scale systems that are essentially discrete. The challenge is therefore to create an integrated multiscale method for modeling and characterization so that deformation mechanisms of a system across several length scales can be captured.

Efforts seeking for multiscale methodologies spanning from atomic to continuum scales can be traced back to the 1970s (e.g., Gehlen et al., 1972). Sinclair's (1975) analytical treatment of the continuum region used a weighted superposition of equilibrium solutions. This method allowed the boundary conditions to be modified during the energy minimization

of the atomic region. The quasi-continuum method has been widely used in multiscale simulations (Tadmor et al., 1996), in which atomic degrees of freedom are selectively removed by interpolating from a subset of representative atoms, similar to the finite element interpolation, and adaptivity criteria are used to reselect these representative lattice points in regions of high deformation. The quasi-continuum method gives a way to bridge the atomic and continuum scales. Another approach is the coupling of FEM with MD. Abraham et al. (1998) used FEM, MD and tight-binding (TB) concurrently in regions of different scales. The FE mesh is graded down to the atomic lattice size in an overlapping (or handshaking) region, and the dynamics is governed by a total Hamiltonian function that combines the separate Hamiltonians of the three regions in a certain way. Since then, various FEM/MD methods based on the handshaking concept have been proposed (Rafii-Tabar et al., 1998; Rudd and Broughton, 1998, 2000; Broughton et al., 1999; Curtin and Miller, 2003).

In many of the existing multiscale modeling methods, the thermal fluctuation is neglected, and therefore, their applications are usually limited to the cases of zero temperature or very low temperature. Recently, some studies on the finite temperature formulations for the multiscale calculation have been reported. Dupuy et al. (2005) developed a coarse-grained (CG) molecular dynamics approach for crystalline solids at constant temperatures in quasi-continuum analyses. Shen and Atluri (2004) added an additional term of the thermal fluctuations in the initial deformation field to derivate an additional random force, which is related to time and temperature and to represent the effects of temperature. The random force can be determined via a probability distribution. Park and Liu (2004) got the similar formulation using the generalized Langevin equation. In addition, Xiao and Belytschko (2004) developed a formulation to consider heat conduction in the multiscale simulation. Although the above methods can partially address the finite temperature issues, there remain many technical problems. Further research is definitely required.

Clearly, the development of the multiscale simulation techniques is still at its infancy, and there are many technical problems remained including:

1) FEM when used for the multiscale analysis is time-consuming and computationally expensive in meshing and re-meshing when solving problems with large deformation, high non-linearity and moving boundaries;

2) A traditional FEM is developed for continuum mechanics based on a discretization mesh, and often causes theoretical and technical problems in ensuring a smooth and seamless transition from the atomic to continuum sub-domains; this becomes more significant when higher order compatibility is required.

Recently, various meshless, or meshfree, approaches have been proposed. Some meshfree methods are based on the strong-forms and the meshfree shape functions, such as the finite point method (Onate et al., 1996) and meshfree collocation method (Wu, 1992). Some meshfree methods are based on global or local weak-forms and meshfree shape functions. Typical examples are the element-free Galerkin (EFG) method (Belytschko et al., 1994), the radial point interpolation method (RPIM) (Liu and Gu, 2001a; Wang and Liu, 2002), the meshless local Petrov-Galerkin (MLPG) method (Atluri et al., 1999; Gu and Liu, 2001), and the local radial point interpolation method (LRPIM) (Liu and Gu,2001b). These methods have demonstrated some distinguished advantages (Liu, 2002; Liu and Gu, 2005):

- They do not use a mesh, so that the burden of mesh generation in FEM is overcome and a smooth atomic-continuum transition becomes possible.
- They are usually more accurate than FEM due to the use of higher order trial functions.
- They are capable of solving complex problems that are difficult for the conventional FEM to apply.

Because of these, meshfree methods seem to have a good potential for multiscale analysis and have attracted the attention of the research community (e.g., Wagner and Liu, 2003; Xiao and Belytschko,2003; Liang and Liu, 2004; Shen and Atluri, 2004). However, the topic is relatively new, and calls for a significant development.

This paper aims to develop a concurrent multiscale simulation technique using the weak-form based meshfree method (i.e., RPIM) to link with a molecular dynamics analysis (abbreviated as the MM method). In the multiscale analysis as shown in Figure 1, a problem domain is divided into a continuum domain Ω^c and an atomic domain Ω^a, but these two domains are joined by a transition one Ω^t. The meshfree RPIM is used for the continuum domain, and MD is used for the atomic domain. The smooth coupling of the mechanics

quantities in these two domains is achieved by the introduction of transition particles which are totally independent of the meshfree field nodes and the MD atoms.

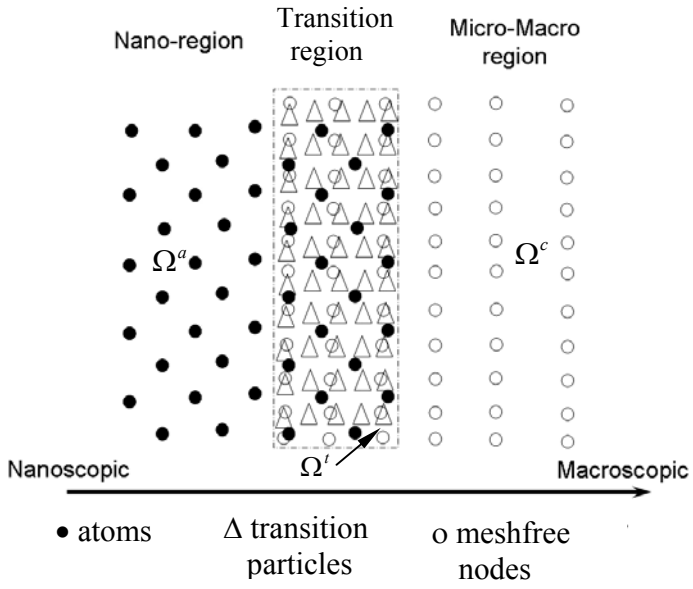

Figure. 1 The handshaking in the transition region

2 Molecular dynamics for the atomic domain

There are several ways to describe an MD analysis, physically (e.g., Zhang and Tanaka, 1997, 1998, 1999) or mathematically (e.g., Rapaport, 1995). For the convenience of a uniform formulation with the meshfree method in this paper, we use the mathematical description below.

In an isolated system composed of atoms or molecules, the system energy keeps constant. The Hamiltonian H^a of a classical atom system is,

$$H^a\left(\mathbf{x}_i,\mathbf{p}_i^a\right)=\sum_i\frac{1}{2m_i^a}\mathbf{p}_i^a\cdot\mathbf{p}_i^a+w^a\left(\mathbf{x}_i\right)=\text{constant} \tag{1}$$

where the superscript a denotes the variable for the atomic domain, m_i^a is the mass of atom i, $\mathbf{x}_i$ is the position of atom i, w^a is the atomic potential, and $\mathbf{p}_i^a$ is the momentum that can be defined by

$$\mathbf{p}_i^a = m_i^a \dot{\mathbf{x}}_i = m_i^a \dot{\mathbf{u}}_i^a \tag{2}$$

where $\mathbf{u}_i^a$ is the displacement of atom *i*. The above equation uses the relation of

$$\mathbf{x}_i = \mathbf{X}_i + \mathbf{u}_i^a \tag{3}$$

where $\mathbf{X}_i$ is the position of atom *i* in the configuration of the system before deformation.

The well-known Hamiltonian canonical equations of the motion are

$$\dot{\mathbf{p}}_i^a = -\frac{\partial H^a\left(\mathbf{x}_i, \mathbf{p}_i^a\right)}{\partial \mathbf{x}_i} = -\frac{\partial w^a}{\partial \mathbf{x}_i} \tag{4}$$

$$\dot{\mathbf{x}}_i^a = \frac{\partial H^a\left(\mathbf{x}_i, \mathbf{p}_i^a\right)}{\partial \mathbf{p}_i^a} = \frac{\mathbf{p}_i^a}{m_i^a} \tag{5}$$

Implying the conservation of energy and the MD trajectories, the Newton's equation of motion can be obtained as

$$m_i^a \ddot{\mathbf{u}}_i^a = \mathbf{f}_i^a = \mathbf{f}_{i(a)}^{\text{ext}} - \mathbf{f}_{i(a)}^{\text{int}} \tag{6}$$

where $\mathbf{f}_{i(a)}^{\text{ext}}$ is the force applied on atom *i* due to a source external to the system such as a body force, often called an external force, and $\mathbf{f}_{i(a)}^{\text{int}} = \partial w^a / \partial \mathbf{u}_i^a$ is the interaction force on atom *i* due to the other atoms in the system, often called an internal force.

3 The meshfree formulation for the continuum domain

3.1 The governing equations

The continuum domain is governed by the conservation of mass, linear and angular momentum, and energy. The conservation of linear momentum (Belytschko et al., 2000) leads to,

$$\frac{\partial P_{ij}}{\partial X_j} + \rho_0 b_i = \rho_0 \ddot{u}_i^c \tag{7}$$

where the superscript *c* denotes the variable for the continuum domain, ρ_0 is the initial density, *P* is the first Piola-Kirchhoff stress tensor, and *b* is the body force.

A body occupies a region ${}_0\Omega$ at the initial (undeformed) stage and occupies a region ${}_t\Omega$ at time *t* after deformation. The deformation of a material particle $\mathbf{X} \in_0 \Omega$ at time *t* can be

described by $\mathbf{x}(\mathbf{X},t) \in_t \Omega$ through a mapping functions $\boldsymbol{\varphi}$ which can be obtained by (Zienkiewicz and Taylor, 2000)

$$\mathbf{x} = \boldsymbol{\varphi}(\mathbf{X},t) = \mathbf{X} + \mathbf{u}^c(\mathbf{X},t) \text{ and } \mathbf{u}^c(\mathbf{X},t) = \mathbf{x}(\mathbf{X},t) - \mathbf{X} \tag{8}$$

where $\mathbf{u}^c$ is the displacement of the material particle. A fundamental measure of deformation is described by the deformation gradient, **F**, relative to **X**, given by

$$\mathbf{F} = \frac{\partial \boldsymbol{\varphi}}{\partial \mathbf{X}} = \frac{\partial \mathbf{x}}{\partial \mathbf{X}} = \frac{\partial \mathbf{u}}{\partial \mathbf{X}} + \mathbf{I}, \text{ and } J = |\mathbf{F}| > 0 \tag{9}$$

3.2 Construction of meshfree shape function

We will use the radial basis function (RBF) interpolation to construct meshfree shape functions, due to its stability and accuracy (Liu, 2002). For a field function, e.g., displacement u, the local RBF interpolation formulation can be written as:

$$u(\mathbf{x}) = \sum_{i=1}^{n} R_i(r) a_i + \sum_{j=1}^{l} p_j(\mathbf{x}) b_j = \mathbf{R}^T \mathbf{a} + \mathbf{B}^T \mathbf{b} = \{\mathbf{R} \quad \mathbf{B}\} \begin{Bmatrix} \mathbf{a} \\ \mathbf{b} \end{Bmatrix} \tag{10}$$

where $R_i(r)$ is the RBF, n is the number of nodes in the interpolation domain of point **x**, $p_j(\mathbf{x})$ is the monomials in the space coordinates $\mathbf{x}^T=[x, y]$, l is the number of polynomial basis functions (usually $n \gg l$), and coefficients a_i and b_j are interpolation constants. The only variable in RBF is the distance r between the interpolation point **x** and a field node $\mathbf{x}_i$, so that the RBF interpolation can be easily extended to three-dimensional problems.

There are a number of RBFs, and characteristics of them have been widely investigated (Powell, 1992; Liu, 2002). In this paper, the following multi-quadrics (MQ) RBF is used based on the local interpolation domains.

$$R_i(\mathbf{x}) = [r_i^2 + (c_0 d_i)^2]^q \tag{11}$$

where c_0 is a dimensionless coefficient, and d_i is a parameter of the nodal spacing. If the nodes are uniformly distributed, d_i is simply the distance between two neighboring nodes (around node i). When nodes are non-uniformly (irregularly) distributed, d_i can be defined as an average nodal spacing in the interpolation domain (Liu, 2002)

These parameters (c_0 and q) determine the performance of the MQ RBF (Liu, 2002; Liu and Gu, 2005). It has been found that c_0=1.0 and q=1.03 lead to good results for a wide class of problems, which will therefore be used in this paper.

In order to determine a_i and b_j in Eq. (10), an interpolation domain is formed for the point of interest at $\mathbf{x}$, and n field nodes are included in this interpolation domain. Coefficients a_i and b_j in Eq. (10) can be determined by enforcing Eq. (10) to be satisfied at these n nodes to lead to n linear equations, one for each node. The matrix form of these equations can be expressed as

$$\mathbf{u}_e = \{u_1 \quad u_2 \quad \cdots \quad u_n\}^{\mathrm{T}} = \mathbf{R}_0\mathbf{a} + \mathbf{B}_m\mathbf{b} \tag{12}$$

where the moment matrix of RBFs, $\mathbf{R}_0$, and the polynomial moment matrix, $\mathbf{B}_m$, are

$$\mathbf{R}_0 = \begin{bmatrix} R_1(r_1) & R_2(r_1) & \cdots & R_n(r_1) \\ R_1(r_2) & R_2(r_2) & \cdots & R_n(r_2) \\ \cdots & \cdots & \cdots & \cdots \\ R_1(r_n) & R_2(r_n) & \cdots & R_n(r_n) \end{bmatrix}, \qquad \mathbf{B}_m^{\mathrm{T}} = \begin{bmatrix} p_1(\mathbf{x}_1) & p_1(\mathbf{x}_2) & \cdots & p_1(\mathbf{x}_n) \\ p_2(\mathbf{x}_1) & p_2(\mathbf{x}_2) & \cdots & p_2(\mathbf{x}_n) \\ \vdots & \vdots & \ddots & \vdots \\ p_l(\mathbf{x}_1) & p_l(\mathbf{x}_2) & \cdots & p_l(\mathbf{x}_n) \end{bmatrix} \tag{13}$$

The vectors of the interpolation coefficients are

$$\mathbf{a}^{\mathrm{T}} = \{a_1 \quad a_2 \quad \ldots \quad a_n\}, \qquad \mathbf{b}^{\mathrm{T}} = \{b_1 \quad b_2 \quad \ldots \quad b_l\} \tag{14}$$

In Eq.(13), r_k in $R_i(r_k)$ is defined as

$$r_k = \sqrt{(x_k - x_i)^2 + (y_k - y_i)^2} \tag{15}$$

However, in Eq. (12), there are only n equations for $n+l$ variables. To obtain unique solution, additional l equations should be added, which are the l constraint conditions, i.e.

$$\sum_{i=1}^{n} p_j(\mathbf{x}_i)a_i = \mathbf{B}_m^{\mathrm{T}}\mathbf{a} = 0, \qquad j=1, 2, \ldots, l \tag{16}$$

Combing Eqs. (12) and (16) yields the following set of equations

$$\tilde{\mathbf{U}}_s = \begin{Bmatrix} \mathbf{u}_e \\ \mathbf{0} \end{Bmatrix} = \begin{bmatrix} \mathbf{R}_0 & \mathbf{B}_m \\ \mathbf{B}_m^{\mathrm{T}} & \mathbf{0} \end{bmatrix} \begin{Bmatrix} \mathbf{a} \\ \mathbf{b} \end{Bmatrix} = \mathbf{G}\mathbf{a}_0 \tag{17}$$

where

$$\mathbf{a}_0^{\mathrm{T}} = \{a_1 \quad a_2 \quad \cdots \quad a_n \quad b_1 \quad b_2 \quad \cdots \quad b_m\} \tag{18}$$

$$\tilde{\mathbf{U}}_s = \{u_1 \quad u_2 \quad \cdots \quad u_n \quad 0 \quad 0 \quad \cdots \quad 0\} \tag{19}$$

From Eq. (17), coefficients $\mathbf{a}_0$ can be solved. The following RBF interpolation formulation is then obtained by substituting $\mathbf{a}_0$ into Eq. (10):

$$u(\mathbf{x}) = \{\mathbf{R}^{\mathrm{T}}(\mathbf{x}) \;\; \mathbf{p}^{\mathrm{T}}(\mathbf{x})\}\mathbf{G}^{-1}\tilde{\mathbf{U}}_s = \tilde{\mathbf{\Phi}}^{\mathrm{T}}(\mathbf{x})\tilde{\mathbf{U}}_s \tag{20}$$

where the augmented RPIM shape functions can be expressed as

$$\begin{aligned}\tilde{\mathbf{\Phi}}^{\mathrm{T}}(\mathbf{x}) &= \{\mathbf{R}^{\mathrm{T}}(\mathbf{x}) \;\; \mathbf{p}^{\mathrm{T}}(\mathbf{x})\}\mathbf{G}^{-1} \\ &= \left\{\Phi_1(\mathbf{x}) \quad \Phi_2(\mathbf{x}) \quad \cdots \quad \Phi_n(\mathbf{x}) \quad \Phi_{n+1}(\mathbf{x}) \quad \cdots \quad \Phi_{n+l}(\mathbf{x})\right\}\end{aligned} \tag{21}$$

Finally, the RPIM shape functions, $\mathbf{\Phi}(\mathbf{x})$, corresponding to the nodal displacements vector, are obtained as

$$\mathbf{\Phi}^{\mathrm{T}}(\mathbf{x}) = \left\{\Phi_1(\mathbf{x}) \quad \Phi_2(\mathbf{x}) \quad \cdots \quad \Phi_n(\mathbf{x})\right\} \tag{22}$$

Eq. (20) can be re-written as

$$u(\mathbf{x}) = \mathbf{\Phi}^{\mathrm{T}}(\mathbf{x})\mathbf{u}_e = \sum_{i=1}^{n} \Phi_i u_i \tag{23}$$

One of the advantages of the RBF shape function is that the meshfree shape functions satisfy the Kronecker delta condition, and therefore, the boundary conditions of a problem can be easily incorporated into the meshfree method. The Kronecker delta function property of the RBF shape function has been proven by Liu (2002). This property can also be easily obtained from the property of the RBF interpolation: the RBF shape functions are created to pass through nodal values (i.e., the interpolated value is the exact same as the nodal value of the sample point when the interpolation point moves to the same position of this sample point). This property is similar to the FEM shape functions, which also have delta property due to passing nodal values in the interpolation.

Similarly, the velocity vector **v** can also be approximated in a similar way, i.e.,

$$\mathbf{v}(\mathbf{X}, t) = \sum_{i=1}^{n} \Phi_i(\mathbf{X})\mathbf{v}_i(t) \tag{24}$$

3.3 Constitutive equation based on an atomic potential

The constitutive equation for the quasi-continuum approach can be constructed using the Cauchy–Born rule (Ericksen, 1984). If $\mathbf{r}_{ij}$ and $\mathbf{R}_{ij}$ are the distances between two atoms *i* and *j*

in the deformed and undeformed configurations, respectively, then they follow the following relationship

$$\mathbf{r}_{ij} = \mathbf{F}\mathbf{R}_{ij} \tag{25}$$

where

$$\mathbf{r}_{ij} = \mathbf{x}_j - \mathbf{x}_i \tag{26}$$

$$\mathbf{R}_{ij} = \mathbf{X}_j - \mathbf{X}_i \tag{27}$$

and $\mathbf{F}$ is the deformation gradient. It should be mentioned that Eq. (25) is only for a simple Bravais lattice that has a centro-symmetric atomic structure. For a complex Bravais lattice, an interpenetration technique using the simple Bravais lattices as sub-lattices needs to be applied to construct an assembly (Zanzotto, 1996). In this case, the Cauchy-Born rule gives (Born and Huang, 1954; Zanzotto, 1996)

$$\mathbf{r}_{ij} = \mathbf{F}\mathbf{R}_{ij} + \boldsymbol{\zeta}_k \tag{28}$$

where $\boldsymbol{\zeta}_k$, independent of $\mathbf{F}$, is a shift vector with k ranging from 0 to an integer M (there are M+1 sub-lattices in the complex Bravais lattice). If atoms i and j are in the same sub-lattice, $\boldsymbol{\zeta}_k = \mathbf{0}$. At a static equilibrium state, $\boldsymbol{\zeta}_k$ can be determined by the minimization of the energy function to reach an equilibrium configuration in the deformed crystal.

The first Piola–Kirchhoff stress can be obtained from

$$\mathbf{P} = \frac{\partial w^{\mathrm{c}}(\mathbf{F})}{\partial \mathbf{F}} \tag{29}$$

where w^{c}, the potential energy per unit volume of the continuum (or strain energy density), will depend on the elongations and angle changes of the atomic bonds and hence underlie the continuum model. Equation (29) is therefore a constitutive equation for a continuum based on atomic potentials.

An important issue now is to get w^{c} based on a known atomic potential w^a. A straightforward way is to sum over potentials (as in the classical molecular dynamics) of all atoms in the continuum domain, i.e.,

$$w^c = \frac{1}{V^c}\sum_i w_i^a \tag{30}$$

where V^c is the volume of a considered continuum domain. However, this method is computationally expensive. A quasi-continuum method (Tadmor et al., 1996; Knap and Ortiz, 2001) has been developed to reduce the computation, based on the finite element and atomic potentials by limiting the summation of the inter-atomic potentials within a single FE element. In the present study, because our meshfree technique for the continuum domain does not have pre-defined elements, we will develop a virtual representative-cell method, as described below, to handle this problem.

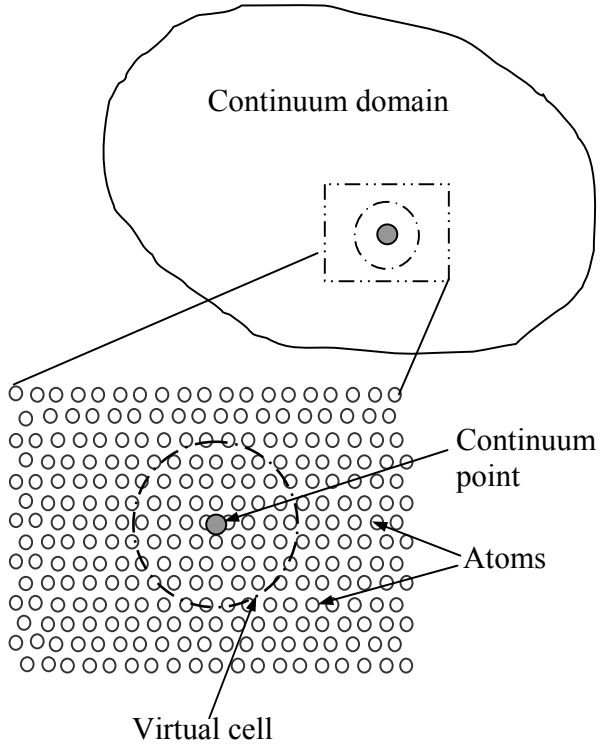

Figure 2. The virtual cell method to get the strain energy density based on the known atomic potentials

As shown in Figure 2, let us consider a point (e.g., the quadrature point or the collocation point) in the continuum domain. A virtual cell, which can be regarded as a large crystallite of a material, can be formed, taking this point as its center. The deformation gradient **F** at this point can be applied to the whole virtual cell to give the continuum energy of the virtual cell

by summing up the energies of all atoms within the cell. The strain energy density for this continuum point can then be obtained as

$$w^c = \frac{1}{V_v^c}\left[\sum_j w_{jv}^a(\mathbf{r}) - \sum_j w_{jv}^a(\mathbf{r}^0)\right] \tag{31}$$

where V_v^c is the volume of the virtual representative-cell (in the undeformed configuration), $w_{jv}^a(\mathbf{r})$ is the potential energy of atom j in the representative-cell when its atomic position moved according to $\mathbf{F}$, and $w_{jv}^a(\mathbf{r}^0)$ is the potential energy of atom j in the unstrained (undeformed) state. $w_{jv}^a(\mathbf{r}^0)$ is constant and does not affect the dynamic analysis.

With the strain energy density obtained above, the first Piola-Kirchhoff stress tensor can be obtained from Eq. (29). We can see that using the virtual representative-cell method, there is no need to take into account the real atomic structure, which makes the simulation efficient.

It should be mentioned here that, in this paper, the examples used assume zero (or very low) temperature, and therefore, the effect of the constant temperature is neglected.

3.4 Meshfree RPIM

Using the Lagrangian approach, the Hamiltonian H^c of a continuum domain can be written as

$$H^c = \int_{\Omega_0^c} \frac{1}{2}\rho \mathbf{v}\cdot\mathbf{v} d\Omega + \int_{\Omega_0^c} w^c(\mathbf{F}) d\Omega \tag{32}$$

where $w^c(\mathbf{F})$ is the energy density due to deformation gradient $\mathbf{F}$, and Ω_0^c is the continuum domain in the initial configuration.

It should be mentioned here that the meshfree radial point interpolation method (RPIM) (Wang and Liu, 2002; Liu and Gu, 2001a) used in this paper is a weak-form based meshfree method, and has been proven to be very stable and accurate (Liu, 2002; Wang and Liu, 2002) for a large class of problems.

For a point *I*, the momentum $\mathbf{p}_I^c$ can be defined by

$$\mathbf{p}_I^c = m_I^c \dot{\mathbf{x}}_I^c = m_I^c \dot{\mathbf{u}}_I^c = m_I^c \mathbf{v}_I^c \tag{33}$$

Using the meshfree RBF interpolation formulation, Eqs. (23) and (24), we can get the following discretized Hamiltonian for the meshfree radial point interpolation method (RPIM).

$$H^c = \sum_I \frac{1}{2m_I^c} \mathbf{p}_I^c \cdot \mathbf{p}_I^c + \int_{\Omega_0^c} w^c(\mathbf{F}) d\Omega \tag{34}$$

Then the Hamiltonian canonical equations of motion can be written as,

$$\dot{\mathbf{p}}_I^c = -\frac{\partial H^c}{\partial \mathbf{x}_I^c} = -\mathbf{f}_{I(c)}^{\text{int}} \tag{35}$$

$$\dot{\mathbf{x}}_I^c = \dot{\mathbf{u}}_I^c = \frac{\partial H^c}{\partial \mathbf{p}_I^c} = \frac{\mathbf{p}_I^c}{m_I^c} \tag{36}$$

The internal force, $\mathbf{f}_{I(c)}^{\text{int}}$, can be obtained by

$$\mathbf{f}_{I(c)}^{\text{int}} = \int_{\Omega_0^c} \frac{\partial w^c}{\partial \mathbf{u}_I^c} d\Omega = \int_{\Omega_0^c} \frac{\partial w^c}{\partial \mathbf{F}} \frac{\partial \mathbf{F}}{\partial \mathbf{u}_I^c} d\Omega = \int_{\Omega_0^c} \frac{\partial w^c}{\partial \mathbf{F}} \frac{\partial (\sum_J \frac{\partial \Phi_J}{\partial \mathbf{X}} \mathbf{u}_J^c + \mathbf{I})}{\partial \mathbf{u}_I^c} d\Omega \tag{37}$$

Considering Eqs. (9) and (29), we can obtain $\mathbf{f}_{I(c)}^{\text{int}}$ from Eq. (37), i.e.,

$$\mathbf{f}_{I(c)}^{\text{int}} = \int_{\Omega_0^c} \frac{\partial w^c}{\partial \mathbf{F}} \frac{\partial \Phi_I}{\partial \mathbf{X}} d\Omega = \int_{\Omega_0^c} \frac{\partial \Phi_I}{\partial \mathbf{X}} \mathbf{P}^c d\Omega \tag{38}$$

Hence, we get the Newton's equation of motion for the continuum domain,

$$m_I^c \ddot{\mathbf{u}}_I = \mathbf{f}_{I(c)}^{\text{ext}} - \mathbf{f}_{I(c)}^{\text{int}} \tag{39}$$

where m_I^c is the mass of node *I*, and $\mathbf{f}_{i(c)}^{\text{ext}}$ is the external force on node *I*.

As mentioned above, we apply the weak-form based meshfree method in the continuum domain. To get the above discrete equations for the continuum domain, the numerical integration is necessary, and the numerical quadrature cells are required. These cells are totally different from the FEM mesh, and they can be very simple and in regular shape (Belytschko et al., 1994; Liu, 2002).

In addition, similar to FEM, a meshfree method can use the consistent ($m = \int \Phi^T \rho_0 \Phi dV$) or a lumped mass matrix. To improve the computational efficiency, we prefer to use the lumped mass matrix in this paper. Based on the quadrature cells, the cell mass, which can be obtained based on the known material density and the cell volume, is assigned to each

meshfree field nodes included in the interpolation for the meshfree shape functions. Hence, we can easily obtain the lumped mass matrix.

4 Atomic-continuum coupling

4.1 Transition technique

As shown in Figure 1, consider a two-dimensional problem domain consisting of a continuum sub-domain Ω^c and an atomic sub-domain Ω^a joined by a transition sub-domain Ω^t that possesses displacement compatibility and force equilibrium in coupling Ω^c and Ω^a. This means that

$$\mathbf{u}_k^c = \mathbf{u}_k^a \tag{40}$$

where $\mathbf{u}_k^c$ and $\mathbf{u}_k^a$ are displacements at a transition particle k obtained by the continuum method and the atomic method, respectively, and that

$$\mathbf{f}_k^c + \mathbf{f}_k^a = 0 \tag{41}$$

where $\mathbf{f}_k^c$ and $\mathbf{f}_k^a$ are forces at a transition particle k computed in Ω^c and Ω^a , respectively.

It will be ideal to satisfy both the displacement compatibility and the force equilibrium conditions of Eqs. (40) and (41), in which the displacement compatibility Eq. (40) is the most important and must be satisfied.

To satisfy the displacement compatibility condition, several handshaking strategies have been developed. Kohlhoff et al. (1991) used a handshaking region between Ω^c and Ω^a, in which the lattice atoms are arranged to coincide with the FEM nodes. To catch the displacement continuity, Ω^c and Ω^a provide the displacement boundary conditions for each other. A bridging algorithm (Wagner and Liu; 2003; Park et al., 2005, Xiao and Belytschko, 2004) has been also developed, which overlays Ω^c and Ω^a at the bridging region. A scaling of the fine and coarse scale potential is used in conjunction with Lagrange multipliers on the overlapping sub-domain. For a seamless multiscale simulation, it is important to ensure that elastic waves generated in Ω^a can propagate into Ω^c. However, the wavelength from Ω^a is often shorter than the nodal spacing in Ω^c so that the short waves from Ω^a are reflected back unphysically from an artificial interface or boundary. To minimize such reflections, some interfacial conditions were proposed (Cai et al.,2000; E and Huang, 2001; Wagner and Liu,

2003). The bridging domain method (Xiao and Belytschko, 2004) was reported to be able to ensure the short wave to cross the interface region with a negligible refection wave. However, in these methods, the continuum nodes and atoms in the interface domain are dependent on each other, which require frequent re-meshing of continuum nodes and bring about computational difficulties. In this paper, following the idea of the bridging domain method, we will develop a new transition technique to ensure a smooth transition between the continuum and atomic sub-domains.

As shown in Figure 1, several layers of transition particles are inserted in the transition domain Ω^t, to ensure the compatibility and facilitate the energy exchange across Ω^a and Ω^c. The displacement compatibility between atoms and meshfree nodes is achieved through these transition particles. The kinetic energy and potential energy of continuum domain will first be transmitted to these transition particles and then to the atomic domain, and *vice versa*.

The advantages of using these transition particles are very clear. First, they allow the meshfree nodes in the continuum domain to have an arbitrary distribution and become independent of the distributions of the atoms in Ω^a. Second, the compatibility conditions in the transition domain can be conveniently controlled through the adjustment of the number and distribution of the transition particles. For some sub-transition domain with stronger compatibility requirement, a finer transition particle distribution can be arranged. In addition, the compatibility of higher order derivatives can also be satisfied.

4.2 Coupling technique

The generalized displacement of a transition particle at $\mathbf{x}_l$ can be defined

$$\mathbf{g}_l = \mathbf{u}^c\left(\mathbf{x}_l\right) - \mathbf{u}^a\left(\mathbf{x}_l\right) \tag{42}$$

where $\mathbf{u}^c(\mathbf{x}_l)$ and $\mathbf{u}^a(\mathbf{x}_l)$ are the displacements of the transition particle at $\mathbf{x}_l$, obtained by the interpolations using the continuum nodes and atoms, respectively, i.e.,

$$\mathbf{u}^c\left(\mathbf{x}_l\right) = \sum_I \mathbf{\Phi}_I\left(\mathbf{x}_l\right)\mathbf{u}_I^c \text{, and } \quad \mathbf{u}^a\left(\mathbf{x}_l\right) = \sum_i \mathbf{\Phi}_i\left(\mathbf{x}_l\right)\mathbf{u}_i^a \tag{43}$$

where $\mathbf{\Phi}$ is the meshfree RBF shape function defined in Eq. (23).

To ensure the conservations of mass and energy, using the method developed by Xiao and Belytschko (2004), the total energy and mass are taken to be linear distributions in the

transition domain. Hence, a scaling parameter, α, as shown in Figure 3, is introduced in the transition region, Ω^t, i.e.,

$$\alpha = \begin{cases} 1, & \mathbf{X} \in \Omega^c - \Omega^t \\ [1,0], & \mathbf{X} \in \Omega^t \\ 0, & \mathbf{X} \in \Omega^a - \Omega^t \end{cases} \tag{44}$$

The Hamiltonian for the total problem domain is the linear combination of the atomic, continuum and the constrain terms of transition particles, i.e.,

$$\begin{aligned} H &= (1-\alpha) H^a + \alpha H^c + H^m \\ &= (1-\alpha) H^a + \alpha H^c + \sum_l \beta_l^{(1)} \mathbf{g}_l + \sum_l \beta_l^{(2)} \mathbf{g}_l^{\mathrm{T}} \mathbf{g}_l \end{aligned} \tag{45}$$

where $\beta_l^{(1)}$ and $\beta_l^{(2)}$ are penalty coefficients for the transition particle *l*.

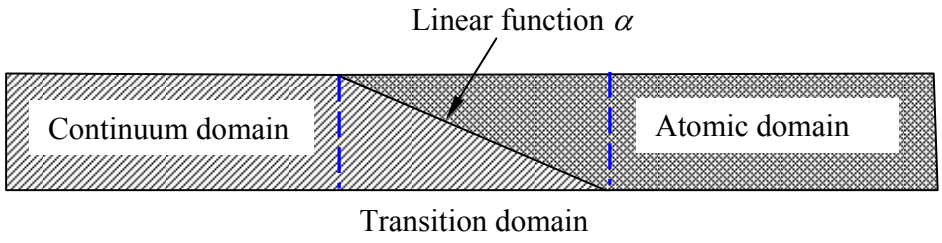

Figure 3. The distributions of mass and energy in the coupled Meshfree/MD method

The Hamiltonian canonical equations of motion are,

$$\begin{aligned} \dot{\mathbf{p}}_I^c &= -\frac{\partial H}{\partial \mathbf{x}_I^c} = -\frac{\partial}{\partial \mathbf{x}_I^c}\left[\alpha H^c + \sum_l \beta_l^{(1)} \mathbf{g}_l + \sum_l \beta_l^{(2)} \mathbf{g}_l^{\mathrm{T}} \mathbf{g}_l \right] \\ &= -\alpha \mathbf{f}_{I(c)}^{\mathrm{int}} - \mathbf{f}_{I(c)}^{\mathrm{tran}} \end{aligned} \tag{46}$$

$$\begin{aligned} \dot{\mathbf{p}}_i^a &= -\frac{\partial H^a}{\partial \mathbf{x}_i^a} = -\frac{\partial}{\partial \mathbf{x}_i^a}\left[(1-\alpha) H^a + \sum_l \beta_l^{(1)} \mathbf{g}_l + \sum_l \beta_l^{(2)} \mathbf{g}_l^{\mathrm{T}} \mathbf{g}_l \right] \\ &= -(1-\alpha) \mathbf{f}_{i(a)}^{\mathrm{int}} - \mathbf{f}_{i(a)}^{\mathrm{tran}} \end{aligned} \tag{47}$$

where $\mathbf{f}_{I(c)}^{\text{tran}}$ and $\mathbf{f}_{i(a)}^{\text{tran}}$ are constraint forces due to the penalty terms to enforce the displacement compatibility condition for the continuum and atomic domain, respectively, i.e.

$$\mathbf{f}_{I(c)}^{\text{tran}} = \sum_l \beta_l^{(1)} \frac{\partial \mathbf{g}_l}{\partial \mathbf{u}_I^c} + \sum_l \beta_l^{(2)} \mathbf{g}_l^{\text{T}} \frac{\partial \mathbf{g}_l}{\partial \mathbf{u}_I^c} \tag{48}$$

$$\mathbf{f}_{i(a)}^{\text{tran}} = \sum_l \beta_l^{(1)} \frac{\partial \mathbf{g}_l}{\partial \mathbf{u}_i^a} + \sum_l \beta_l^{(2)} \mathbf{g}_l^{\text{T}} \frac{\partial \mathbf{g}_l}{\partial \mathbf{u}_i^a} \tag{49}$$

Substituting Eqs. (42) and (43) into Eqs. (48) and (49), we can get the discrete formulations of $\mathbf{f}_{I(c)}^{\text{tran}}$ and $\mathbf{f}_{i(a)}^{\text{tran}}$

$$\mathbf{f}_{I(c)}^{\text{tran}} = \sum_l \beta_l^{(1)} \Phi_{Il} \mathbf{I} + \sum_l \beta_l^{(2)} \left[\sum_I \Phi_I(\mathbf{x}_l) \mathbf{u}_I^c - \sum_i \Phi_i(\mathbf{x}_l) \mathbf{u}_i^a \right] [\Phi_{Il} \mathbf{I}] \tag{50}$$

$$\mathbf{f}_{i(a)}^{\text{tran}} = -\sum_l \beta_l^{(1)} \Phi_{il} \mathbf{I} - \sum_l \beta_l^{(2)} \left[\sum_I \Phi_I(\mathbf{x}_l) \mathbf{u}_I^c - \sum_i \Phi_i(\mathbf{x}_l) \mathbf{u}_i^a \right] [\Phi_{il} \mathbf{I}] \tag{51}$$

The equations of motions of this coupling system can be written as

$$m_I^c \ddot{\mathbf{u}}_I^c = \mathbf{f}_I^c = \mathbf{f}_{I(c)}^{\text{ext}} - \left(\mathbf{f}_{I(c)}^{\text{int}} + \frac{\mathbf{f}_{I(c)}^{\text{tran}}}{\alpha(\mathbf{X}_I)} \right) \tag{52}$$

$$m_i^a \ddot{\mathbf{u}}_i^a = \mathbf{f}_i^a = \mathbf{f}_{i(a)}^{\text{ext}} - \left(\mathbf{f}_{i(a)}^{\text{int}} + \frac{\mathbf{f}_{i(a)}^{\text{tran}}}{1-\alpha(\mathbf{X}_i)} \right) \tag{53}$$

The above Newton's equations of motion are often solved by Velocity Verlet integrator, i.e.,

$$\mathbf{u}_{i(n+1)} = \mathbf{u}_{i(n)} + \dot{\mathbf{u}}_{i(n)} \Delta t + \frac{1}{2} \frac{\mathbf{f}_{i(n)}}{m_i} \Delta t^2 \tag{54}$$

$$\dot{\mathbf{u}}_{i(n+1)} = \dot{\mathbf{u}}_{i(n)} + \left(\mathbf{f}_{i(n)} + \mathbf{f}_{i(n+1)} \right) \frac{\Delta t}{2 m_i} \tag{55}$$

To satisfy the force equilibrium condition, the generalized derivative at a transition particle $\mathbf{x}_l$ is

$$\mathbf{g}_{l(\mathbf{x})} = \frac{\partial \mathbf{u}^c(\mathbf{x}_l)}{\partial \mathbf{x}^c} - \frac{\partial \mathbf{u}^a(\mathbf{x}_l)}{\partial \mathbf{x}^a} \tag{56}$$

We can get the discrete formulations of the additional forces of $\mathbf{f}_{I(c)}^{\text{tran}(\mathbf{x})}$ and $\mathbf{f}_{i(a)}^{\text{tran}(\mathbf{x})}$

$$\mathbf{f}_{I(c)}^{\text{tran}(\mathbf{x})} = \sum_l \beta_l^{(3)} \Phi_{Il,\mathbf{x}} \mathbf{I} \tag{57}$$

$$\mathbf{f}_{i(a)}^{\text{tran}(\mathbf{x})} = -\sum_l \beta_l^{(3)} \Phi_{il,\mathbf{x}} \mathbf{I} \tag{58}$$

where $\beta_l^{(3)}$ is penalty coefficients for the transition particle *l*.

Hence, the equations of motion, Eqs. (54) and (55), can be re-written as

$$m_I^c \ddot{\mathbf{u}}_I^c = \mathbf{f}_I^c = \mathbf{f}_{I(c)}^{\text{ext}} - \left(\mathbf{f}_{I(c)}^{\text{int}} + \frac{\mathbf{f}_{I(c)}^{\text{tran}} + \mathbf{f}_{I(c)}^{\text{tran}(\mathbf{x})}}{\alpha(\mathbf{X}_I)} \right) \tag{59}$$

$$m_i^a \ddot{\mathbf{u}}_i^a = \mathbf{f}_i^a = \mathbf{f}_{i(a)}^{\text{ext}} - \left(\mathbf{f}_{i(a)}^{\text{int}} + \frac{\mathbf{f}_{i(a)}^{\text{tran}} + \mathbf{f}_{i(a)}^{\text{tran}(\mathbf{x})}}{1-\alpha(\mathbf{X}_i)} \right) \tag{60}$$

The penalty coefficients β_i are usually different from problem to problem. However, there is usually a range for the selection of the penalty coefficients. For the examples in Section 5, our studies had found that $\beta_i = \alpha \cdot (m_{ii})_{\max}$ (where $\alpha = 10 \sim 10^3$, and $(m_{ii})_{\max}$ is the maximum diagonal element of the mass matrix) lead to satisfactory results. A more accurate method is so called the Lagrange multiplier method, which considers the penalty coefficients as also variables λ_i (not constants). Additional equations are obtained and solved together with the system equations to bring about the Lagrange multipliers (i.e. special penalty coefficients). The advantages of the Lagrange multiplier method include: 1) no pre-determined penalty coefficients, and 2) more accurate. However, it will increase the computational cost (especially when the number of transition particles is large) because new variables (Lagrange multipliers) are added. Hence, we can use the Lagrange multiplier method to obtain a range of penalty coefficients, and then use them as constants for this problem and other similar problems.

4.3 Multiple-time-step algorithm

Since the frequency of the atomic domain is much higher than that of the continuum domain, a single time step for both continuum and atomic domains is unwise. Multiple-time-step algorithm is more favorable, both computationally and physically. Hence, the multiple-time-

step algorithm is often used in the multiscale modelling (Xiao and Belytschko, 2004). We will use a larger time step in the continuum sub-domain but a finer time step in the atomic sub-domain. If ΔT^c is the time step in the continuum sub-domain and Δt^a that in the atomic sub-domain, we can use

$$\Delta T^c = N\Delta t^a \tag{61}$$

where $N > 0$ is an integer to be determined.

Therefore, the Velocity Verlet integrator can be rewritten as,

$$\mathbf{u}_{I(n+1)} = \mathbf{u}_{I(n)} + \dot{\mathbf{u}}_{I(n)}\Delta T + \frac{1}{2}\frac{\mathbf{f}_{I(n)}}{m_I^c}\Delta T^2, \text{ in } \Omega^{\mathrm{c}} \tag{62}$$

$$\mathbf{u}_{i\left(n+\frac{j+1}{N}\right)} = \mathbf{u}_{i\left(n+\frac{j}{N}\right)} + \dot{\mathbf{u}}_{i\left(n+\frac{j}{N}\right)}\Delta t + \frac{1}{2}\frac{\mathbf{f}_{i\left(n+\frac{j}{N}\right)}}{m_i^a}\Delta t^2, \text{ in } \Omega^{\mathrm{a}} \tag{63}$$

and

$$\dot{\mathbf{u}}_{I\left(n+\frac{j+1}{N}\right)} = \dot{\mathbf{u}}_{I\left(n+\frac{j}{N}\right)} + \frac{\Delta t}{2m_I^c}\left(\mathbf{f}_{I\left(n+\frac{j}{N}\right)} + \mathbf{f}_{I\left(n+\frac{j+1}{N}\right)}\right), \text{ in } \Omega^{\mathrm{c}} \tag{64}$$

$$\dot{\mathbf{u}}_{i\left(n+\frac{j+1}{N}\right)} = \dot{\mathbf{u}}_{i\left(n+\frac{j}{N}\right)} + \frac{\Delta t}{2m_i^a}\left(\mathbf{f}_{i\left(n+\frac{j}{N}\right)} + \mathbf{f}_{i\left(n+\frac{j+1}{N}\right)}\right), \text{ in } \Omega^{\mathrm{a}} \tag{65}$$

where $j = 0 \sim N-1$. The above equations mean that the variables in the atomic domain will be repeatedly calculated for N times at the finer time step to match the coarse time step in the continuum domain.

4.4 The flowchart

With the above formulation, the multi-scale simulation can be carried out the following flowchart in Table 1.

Table 1 The flowchart of the multiscale analysis

1. Input geometry, meshfree nodes, transition particles, atoms, external forces, boundary conditions, and other coefficients;
2. Give the initial conditions;
3. Calculate meshless shape functions for all Gauss points using Eq. (23);
4. Calculate interpolation functions for all transition particles using Eq. (23);
5. Loop when the time step is smaller than the given number
   5.1 Loop from 1 to N ($\Delta T = N\Delta t$)
      5.1.1 Calculate the force for atoms from the atomic potential;
      5.1.2 Calculate the constraint forces for atoms using Eqs. (51) and (58);
      5.1.3 Update positions and velocities of atoms using Eqs. (63) and (65);
      5.1.4 Update velocities for meshfree nodes using Eq. (64);
      5.1.5 End loop 5.1;
   5.2 Calculate the first Piola-Kirchhoff stress vectors for meshfree nodes using Eq. (29);
   5.3 Calculate the constraint forces for meshfree nodes using Eqs. (50) and (57);
   5.4 Update positions for meshfree nodes using Eq. (62);
   5.5 Calculate energy and other statistical values;
   5.6 Output results for selected time steps;
   5.7 End loop 5.
6. Output results.
7. End

5 Results and discussion

Here, we will investigate several examples to demonstrate the effectiveness of the present multiscale simulation method. We will use five closest field nodes for one-dimensional problems, and sixteen closest field nodes for two-dimensional problems, to construct the meshfree RBF shape functions. It should be mentioned here that how to select suitable nodes to perform the meshfree interpolation is a key issue in the use of a meshfree method, and it is still an open problem. Fortunately, for most problems with no severe nodal irregularity, using the distance criterion is simple and appropriate, in which the nodal distance should be based on the "average" nodal spacing (Liu, 2002).

5.1 One-dimensional chain

Consider the wave propagation in a one-dimensional chain whose two ends are traction free (Wagner and Liu, 2003; Huang and Liu, 2005). We use the harmonic potential

$$w^a\left(r_{ij}\right) = \frac{1}{2}k\left(r_{ij}^a - r_0^a\right)^2 \tag{66}$$

in the atomic sub-domain, where k is the spring stiffness, r_{ij}^a is the inter-atomic distance and r_0^a is the equilibrium bond length. In the continuum sub-domain, the virtual representative-cell method given in Section 3.3 is used to obtain the first Piola–Kirchhoff stress. The coupling model for this 1-D problem is shown in Figure 4. The length of this chain is 30 nm. In the continuum sub-domain, 26 meshfree nodes are used, and the distance between two nodes is $r_0^c = 0.8$ nm. The atomic sub-domain contains 71 atoms with an atomic distance $r_0^a = 0.2$ nm. The length of the atomic-continuum transition region is 4nm, containing 35 transition particles. An initial displacement, applied on the left portion of the continuum sub-domain (4.0 nm), is taken as one-quarter of sinusoid. The time step for the atomic domain is Δt^a=0.01ps so that the time step in the continuum sub-domain is $\Delta T^c = N\Delta t^a$. The initial N is 5 (the effect of N will be discussed later.) For comparison, the problem is also simulated by only MD and the relative error between the MD and our multiscale results is measured by the following error indicator

$$e = \frac{\left| \sum_i^m \left| u_i^{\mathrm{MD}} \right| - \sum_i^m \left| u_i^{\mathrm{MM}} \right| \right|}{\sum_i^m \left| u_i^{\mathrm{MD}} \right|} \tag{67}$$

where u_i^{MD} and u_i^{MM} are displacement at the ith atom in the atomic domain obtained using the MD and our MM method, respectively; m is the number of atoms in the atomic sub-domain.

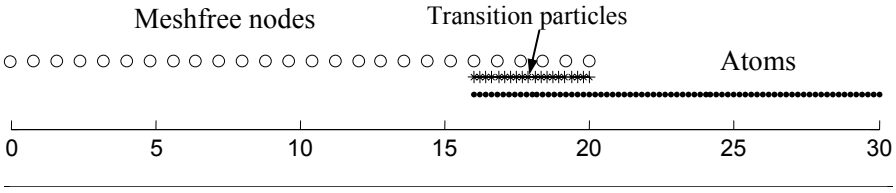

Figure 4. The computational model for 1-D wave propagation problem

Figures 5 and 6 show the displacements, obtained by MD and MM at different time steps. It can be seen that the MM method leads to almost identical results with those from MD. The

relative errors in Figure 7 indicate that the present MM method is more accurate than that using the coupling of FEM and MD.

Figure 8 shows the energy (the sum of kinetic and potential energies) transfer between the continuum and atomic sub-domains. It is clear that almost all energy in the continuum sub-domain has been transferred to the atomic sub-domain. This means that the transition algorithm we developed in this paper can ensure an excellent energy transfer while satisfying the compatibility conditions.

Errors for different multiple time-step coefficient, N, are demonstrated in Figures 9 and 10. It can be found that the computational errors increase only slightly with the increase of N when $N \le 20$. However, the errors will significantly increase when $N > 20$. This suggests that an appropriate N is important. It is understandable that a too large N cannot be good, because the accuracy for energy transfer and compatibility in transition will become worse. In addition, if the time step is larger than the critical time step (mainly determined by the nodal spacing for the meshfree field nodes) for the continuum domain, the computational error will increase significantly, or even fail. For this problem, N =5~15 is a good choice.

The average errors for different numbers of transition particles are illustrated in Figure 11, where we can see that the computational results are stable when the number is large enough (>5 for this problem). Too few transition particles cannot ensure the compatibility accuracy, and hence lead to a large computational error. On the other hand, if the transition particles are too many, it will significantly increase the computational time without noticeable accuracy improvement. Hence, the number of transition particles should be considered to maximise the computation efficiency with acceptable accuracy. For the present example, 15~35 particles are a good selection.

5.2 Two-dimensional grapheme sheet

Here we examine the wave propagation in a two-dimensional grapheme sheet whose thickness is a single atom layer. The following Lennard-Jones (L-J) 6-12 lnteratomic potential (Girifalco and Lad, 1956) is used

$$w^a(\mathbf{r}_{ij}) = 4\varepsilon\left[\left(\frac{\sigma}{\mathbf{r}_{ij}}\right)^{12} - \left(\frac{\sigma}{\mathbf{r}_{ij}}\right)^{6}\right] \tag{68}$$

in the atomic sub-domain with $\varepsilon = 0.2J$ and $\sigma = 0.11\text{nm}$. The inter-atomic force for bond $\mathbf{r}_{ij}$ is the negative of the first derivative of the potential with respect to $\mathbf{r}_{ij}$, i.e.

$$\mathbf{f}_{ij}^a = -\nabla\Phi = \frac{48\varepsilon\mathbf{r}_{ij}}{\sigma^2}\left[\left(\frac{\sigma}{\mathbf{r}_{ij}}\right)^{14} - \frac{1}{2}\left(\frac{\sigma}{\mathbf{r}_{ij}}\right)^{8}\right] \tag{69}$$

The initial displacement is taken as a quarter of sinusoid, and applied on the right portion of the atomic domain. The periodic boundary condition is applied along the vertical direction. The coupling model of this 2-D sheet is shown in Figure 12 with 8.3098 nm in length and 0.9624 nm in width, containing 420 atoms in the atomic sub-domain, and 110 regularly distributed meshfree field nodes in the continuum sub-domain. The length of the transition region is 1.95 nm, containing 300 transition particles. The time step for the atomic domain is Δt^a=0.005ps, and the multiple time step factor N is 5 (i.e., $\Delta T^c = 5\Delta t^a = 0.025\text{ps}$).

Figures 13 and 14 show the displacements, obtained by MD and MM methods respectively. It can be found that the presently developed MM method leads to almost identical results with those from MD. Figure 15 shows the energy transfer between the continuum and atomic sub-domains. It demonstrates that all the energy in atomic sub-domain has been transferred into the continuum sub-domain through our transition technique.

To study the effectiveness of the multiscale method for the irregularly distributed continuum nodes, 163 irregular continuum nodes, as shown in Figure 16, are used in the continuum domain, and the same atoms and transition particles are used in the atomic domain and the transition domain. Figure 17 shows the displacements, obtained by MD and MM methods respectively. The comparison shows that the MM method using the irregular nodes leads to very good results.

5.3 Cylindrical wave propagation

In this example, we use the harmonic potential in the cylindrical wave propagation problem in a square domain (Liang and Liu, 2004). The computational model is shown in Figure 18. Due

to the symmetry of the problem, only the right part of the square sheet is plotted. We use 1312 meshfree nodes in the continuum sub-domain, and 8400 atoms in the atomic sub-domain. The two horizontal ends are traction free, and the periodic boundary condition is applied along the vertical direction. The length of the transition sub-domain is 2 nm, containing 972 transition particles.

Figure 19 shows that the cylindrical wave from the atomic sub-domain travels to the continuum sub-domain well, proving that our MM method and transition technique can ensure the smooth propagation of elastic waves generated in the atomic sub-domain into the continuum sub-domain. Compared with results obtained by other researchers (Liang and Liu, 2004), we can see that the present MM method lead to more accurate results.

The irregularly distributed continuum nodes are also used for this problem. Figure 20 shows a computational model using 636 irregular continuum nodes in the continuum domain. It has been found that the MM method with irregular nodes leads to almost identical results with those from MM with regular nodes. Again, it proves that the present MM method is very effective for the analysis with irregular continuum nodes.

6 Conclusion

This paper has developed a concurrent multiscale method based on the weak-from based meshfree RPIM method and molecular dynamics with a successful transition technique. The numerical examples have demonstrated that the method gives more accurate results compared with others. The main advantages of the new method are as follows:

a) It avoids mesh generation and hence can be used to solve many special problems that are difficult for others relying on the finite element method.
b) It is computationally more accurate since the meshfree RPIM has a higher accuracy than the FEM.
c) The transition region from atomic to continuum sub-domain in the present method can be constructed more easily because no nodal continuity is required in the meshfree method.
d) The transition particles can have an arbitrary distribution and are independent of the distributions of the meshfree nodes in the continuum sub-domain and the atoms in the atomic sub-domain. The compatibility conditions in the transition domain can be

conveniently controlled through the adjustment of the number and distribution of transition particles.

e) The compatibility requirement for higher order derivatives can be easily satisfied.

It has been found that the multiple-time step factor N and the number of particles in the transition region will influence the simulation accuracy. Although the best values of them for the problems studied in this paper have been obtained, the rational optimisation of these parameters needs a further investigation.

Acknowledgement

This work was supported by an ARC Discovery Grant.

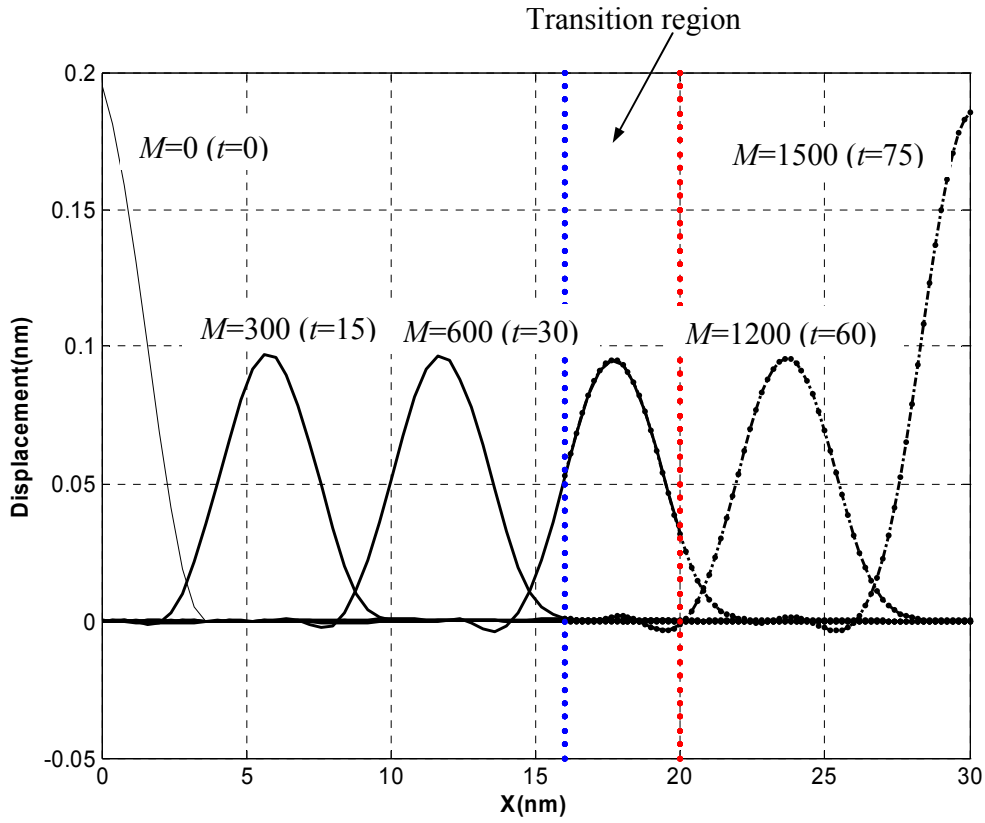

Figure 5. Displacements at different time steps obtained by the coupled meshfree/MD method (M is the number of time steps) ($\Delta T^c = 5\Delta t^a$)

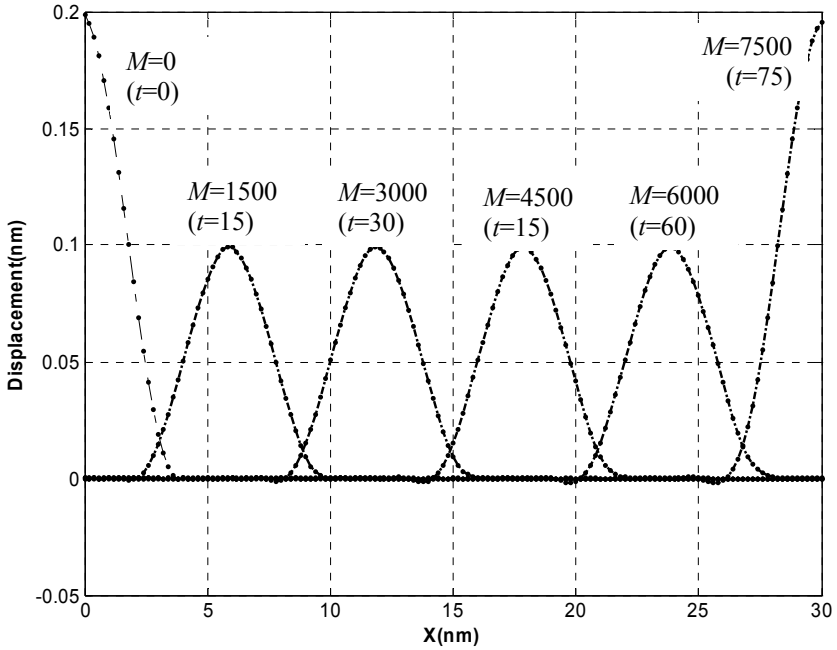

Figure 6. Displacements at different time steps obtained by the purely MD

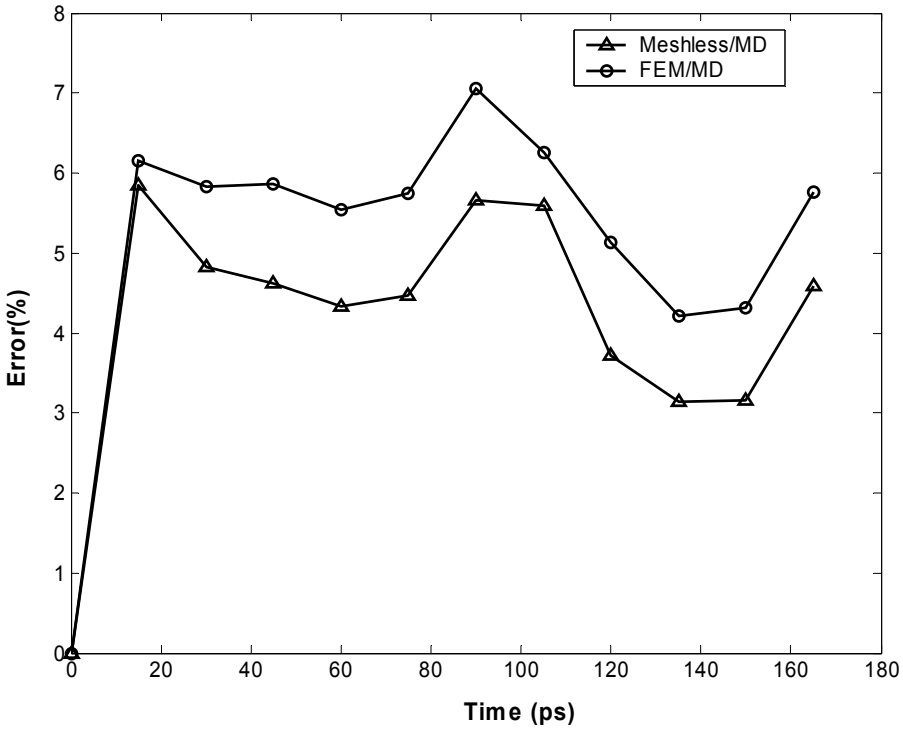

Figure 7. Computational errors ($\Delta T^c = 5\Delta t^a$)

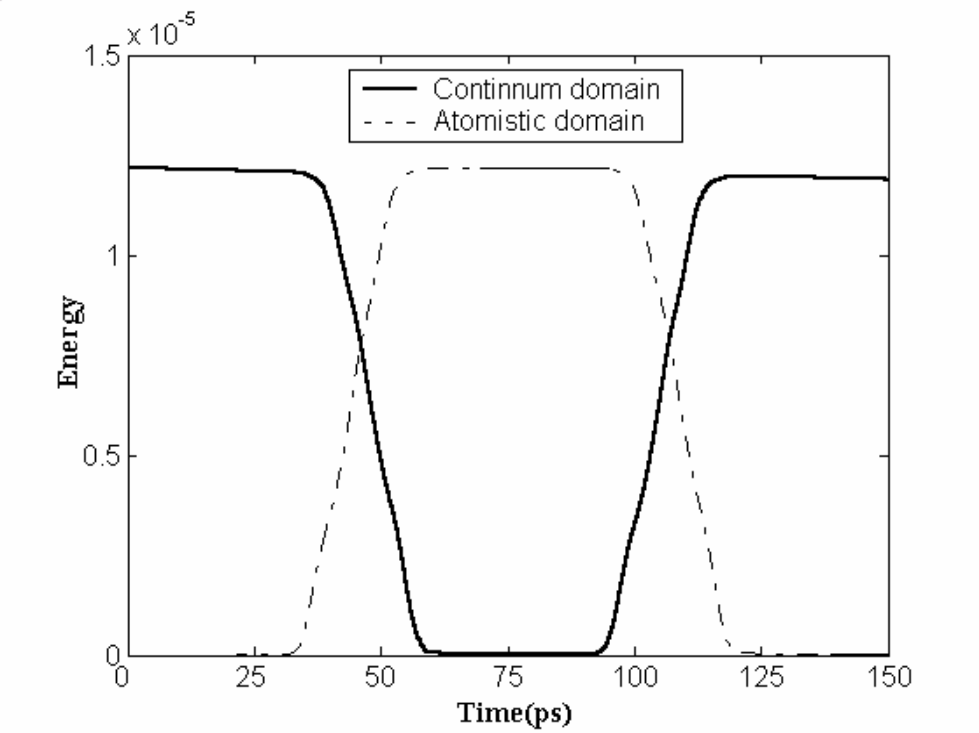

Figure 8. Energy transfer between the continuum and atomic domains ($\Delta T^c = 5\Delta t^a$)

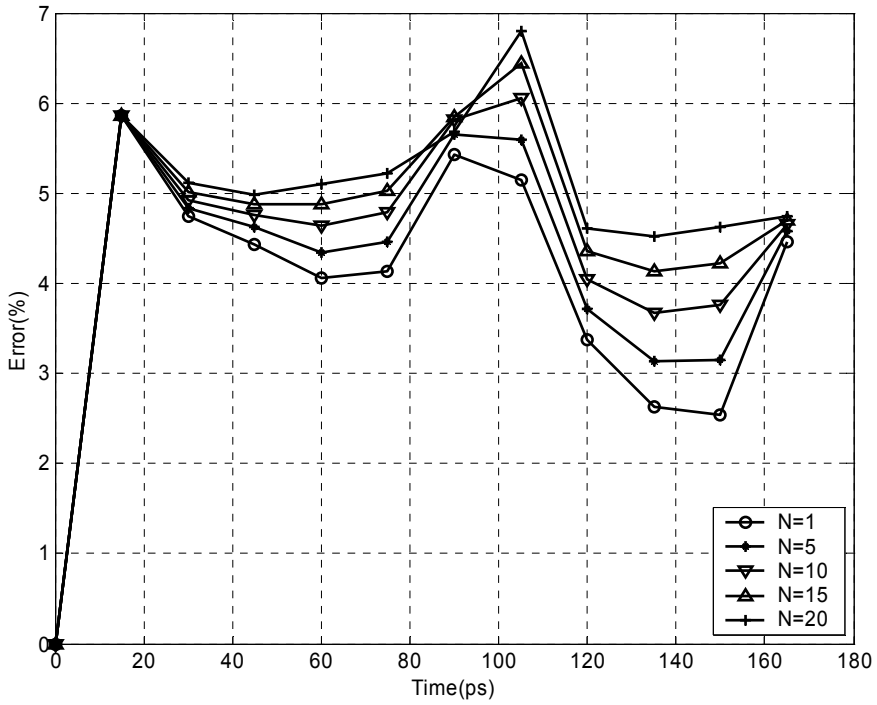

Figure 9. Computational errors for different multiple-time step factor N ($\Delta T^c = N\Delta t^a$)

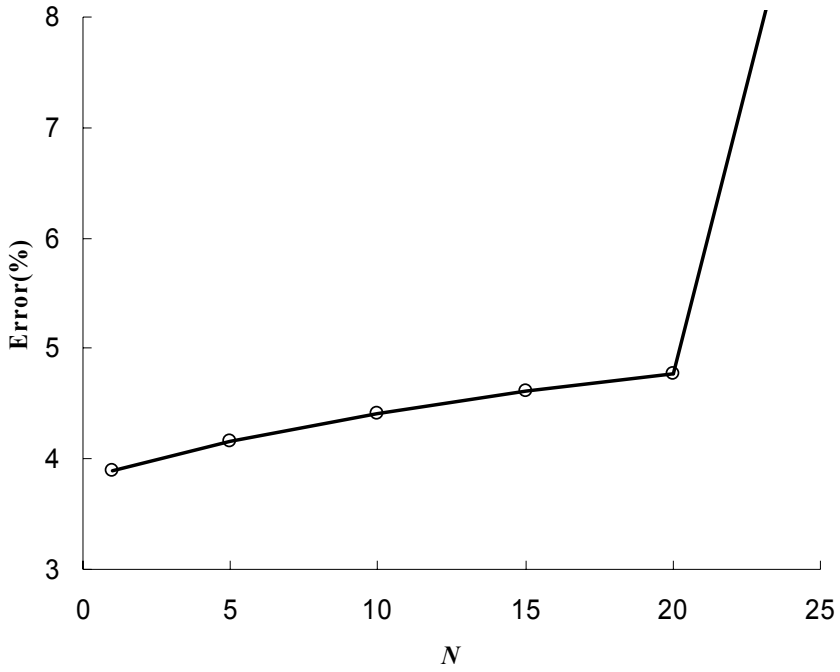

Figure 10. Average computational errors for different multiple-time step factor N ($\Delta T^c = N\Delta t^a$)

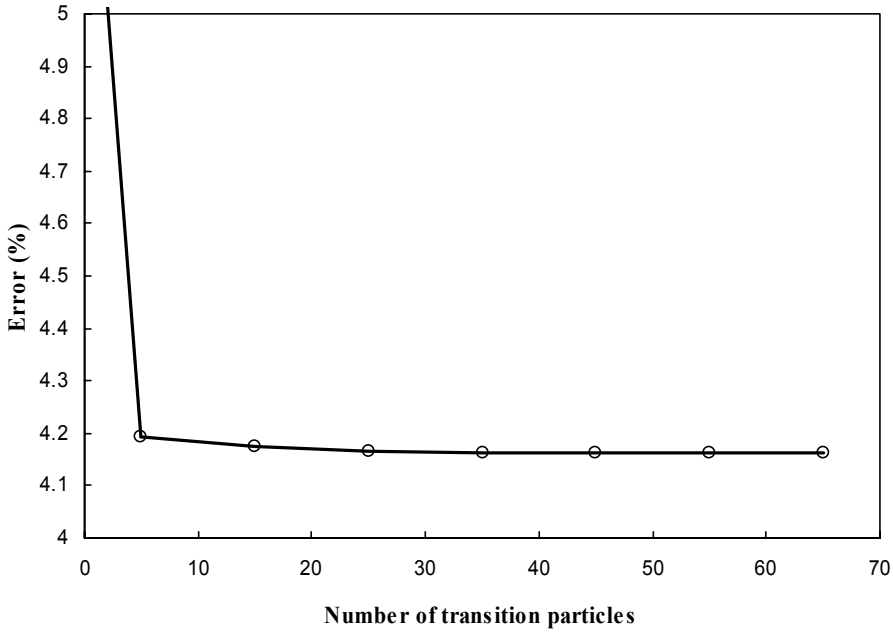

Figure 11. Average computational errors for different numbers of transition particles ($\Delta T^c = 5\Delta t^a$)

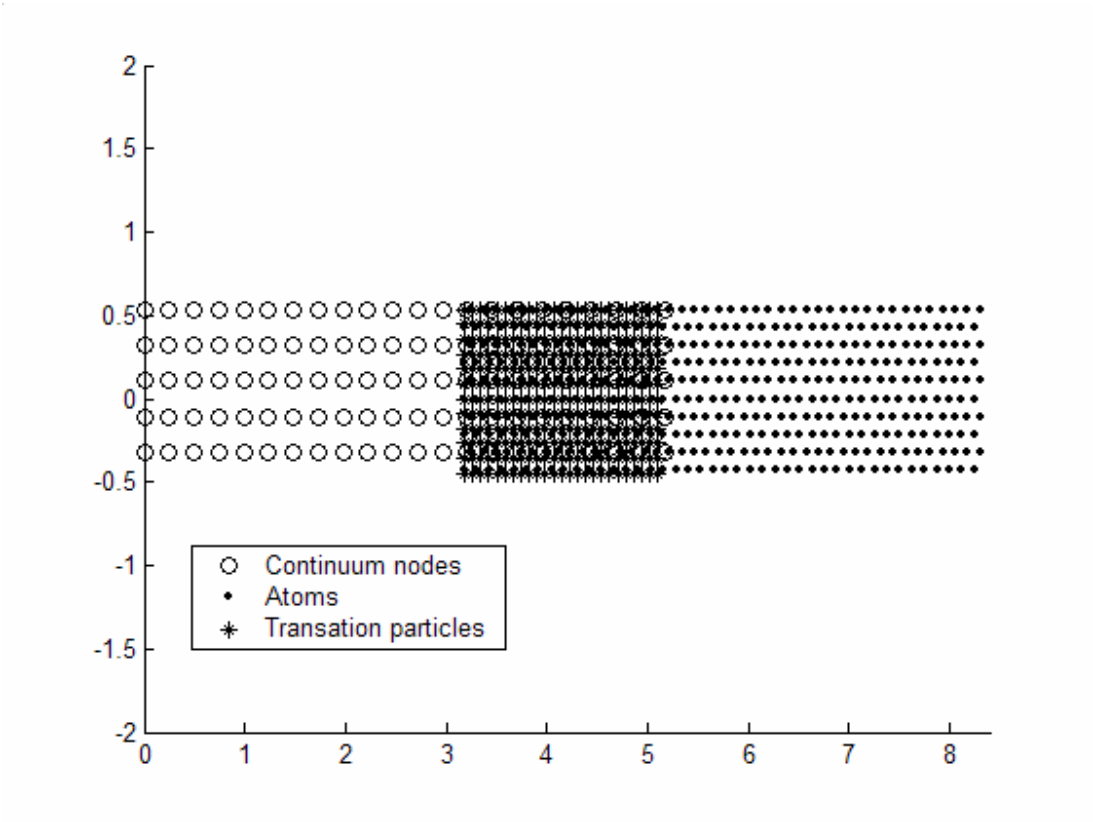

Figure 12. The computational model for 2-D wave propagation problem

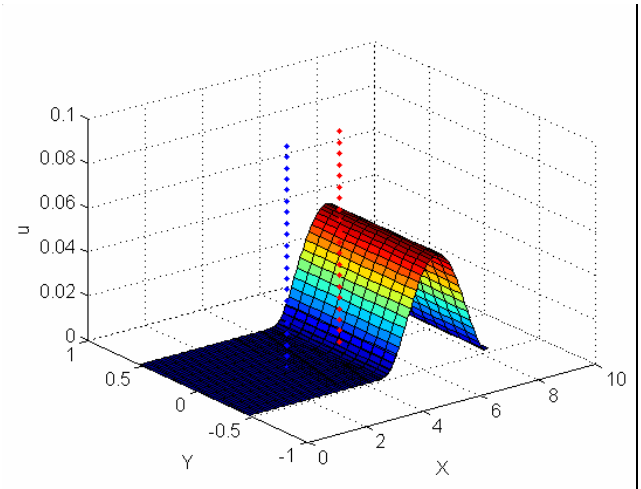

(a) Meshfree/MD (t=0.5 ps)

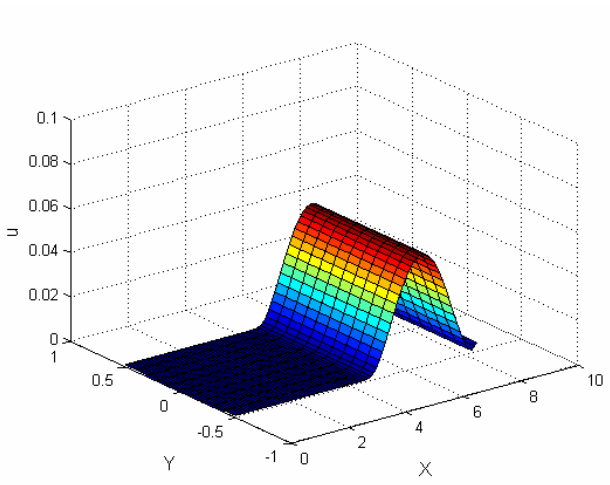

(d) MD (t=0.5 ps)

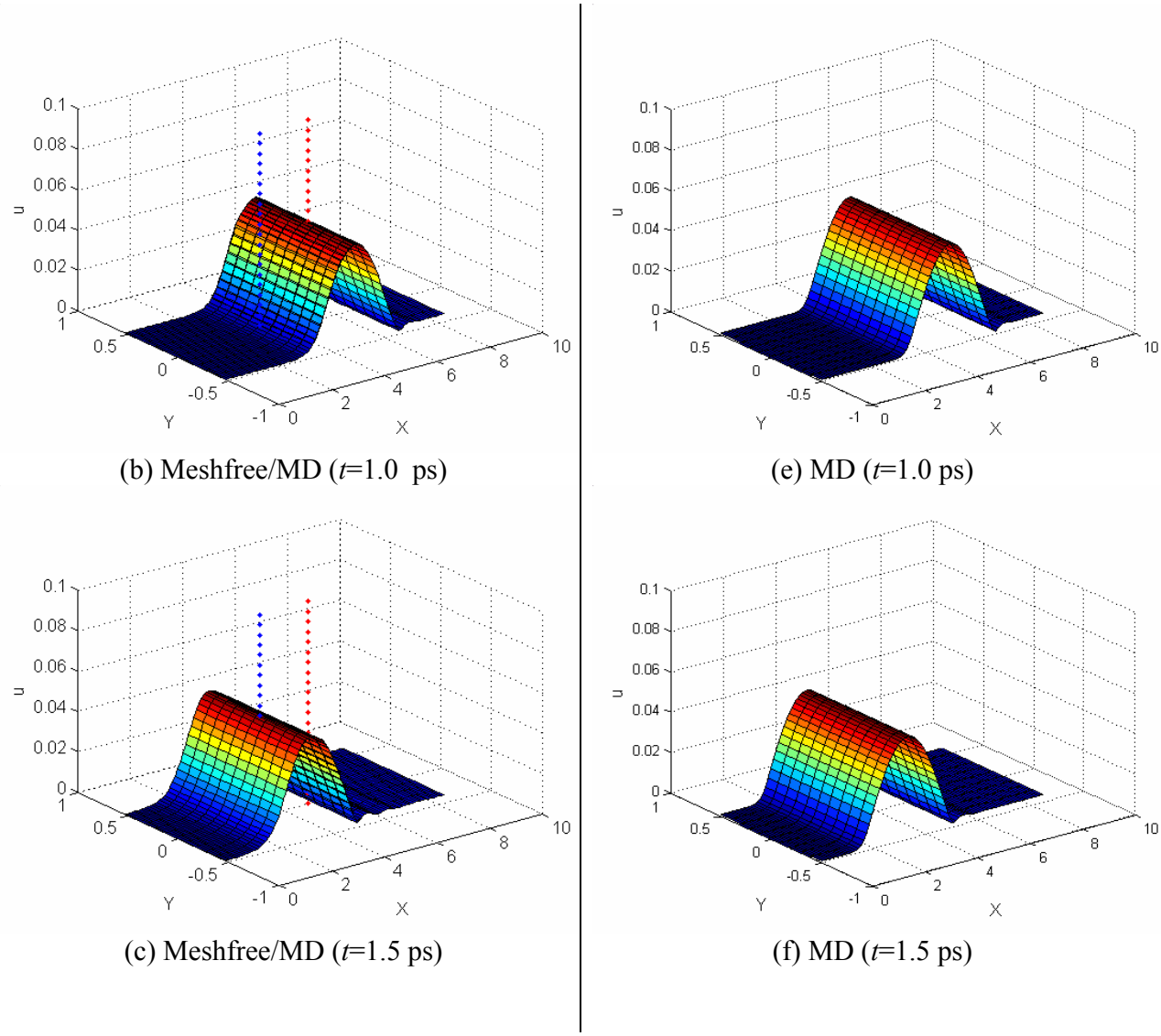

(b) Meshfree/MD (t=1.0 ps)

(e) MD (t=1.0 ps)

(c) Meshfree/MD (t=1.5 ps)

(f) MD (t=1.5 ps)

Figure 13. Displacements at different time steps obtained by the coupled MM method and the purely MD (between two dot lines is the transition domain). It shows that the coupled MM method leads to almost identical results with MD.

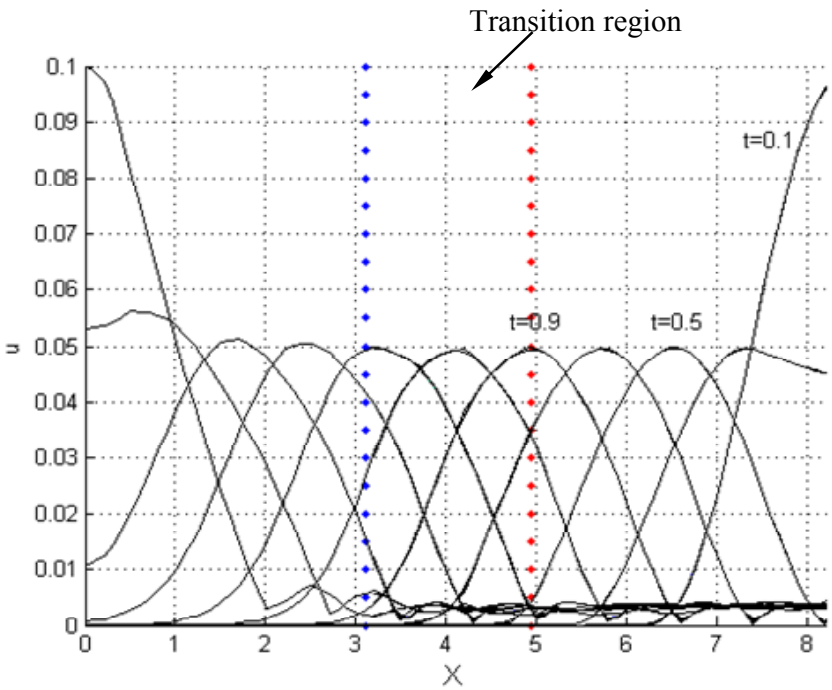

Figure 14. Displacements at different time steps obtained by the coupled meshfree/MD method and in the view of *x*-*u*

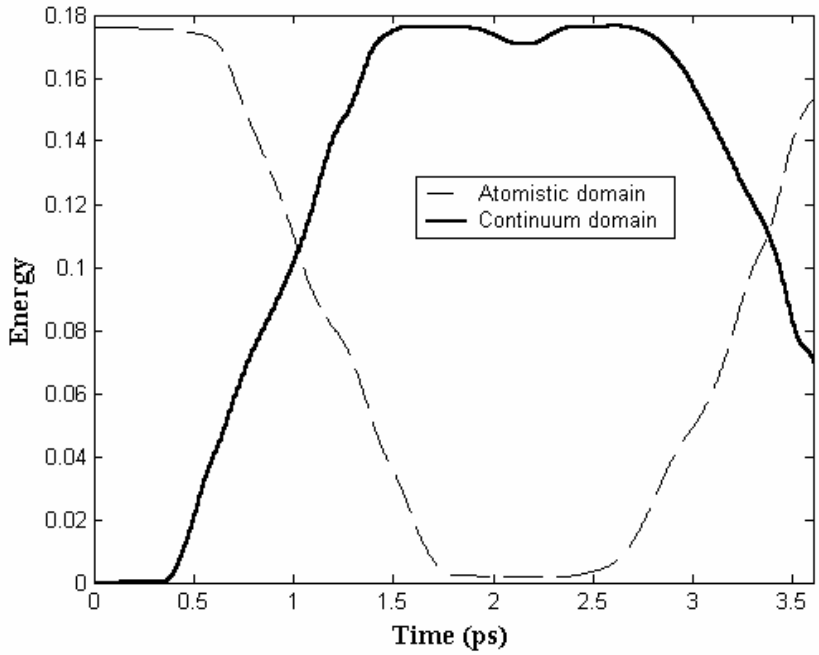

Figure 15. Energy transfer between the continuum and atomic domains for the 2-D problem ($\Delta T^c = 5\Delta t^a$)

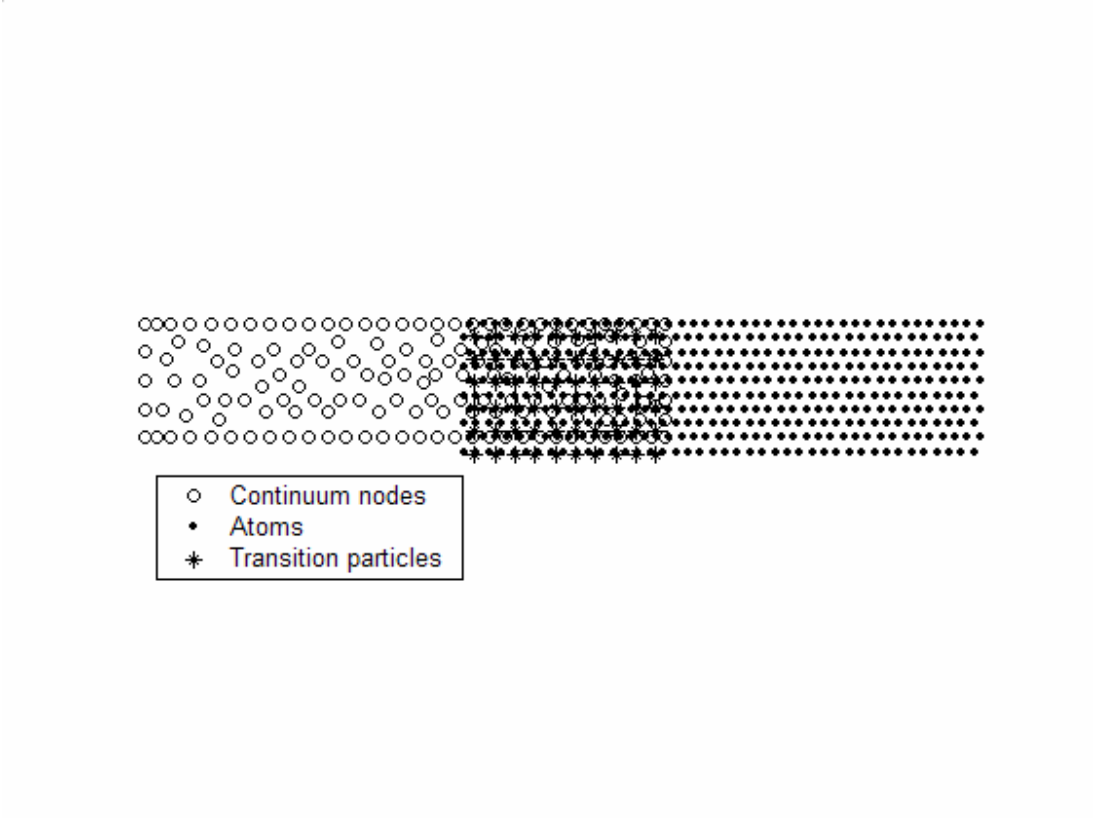

Figure 16. The computational model for 2-D wave propagation problem using irregularly distributed 163 continuum nodes (the irregular nodes are generated using the MFree 2D® (Liu, 2002) software package)

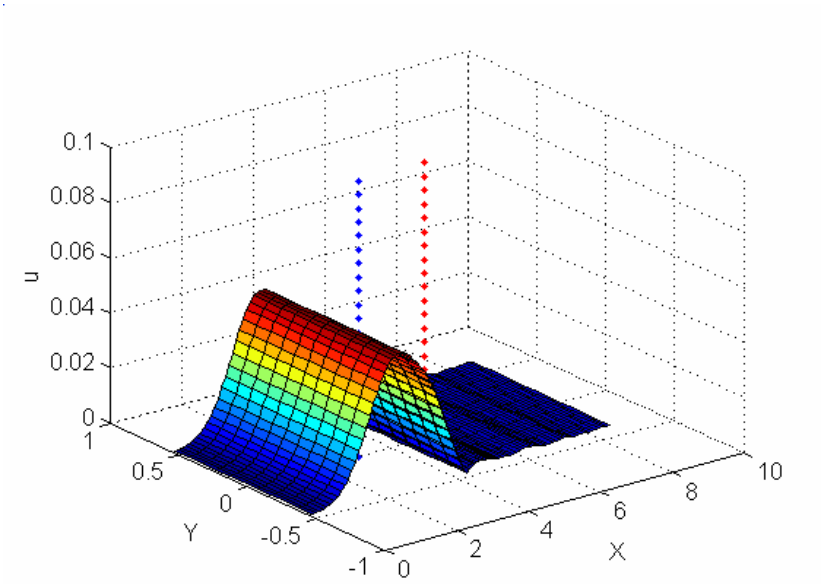

(a) Meshfree/MD (t=1.5 ps)

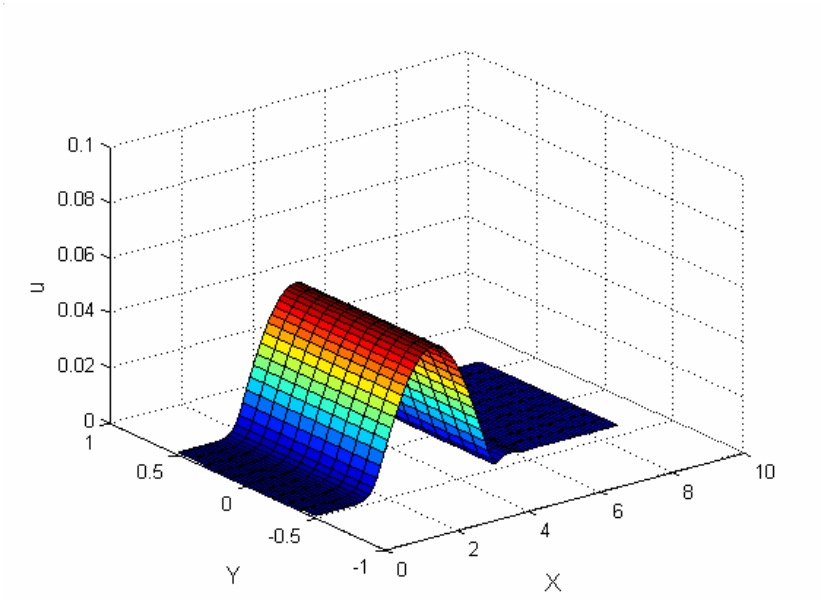

(b) MD (t=1.5 ps)

Figure 17. Displacements obtained by the MM method using the irregular continuum nodes and the purely MD (between two dot lines is the transition domain). It shows that the coupled MM method leads to almost identical results with MD.

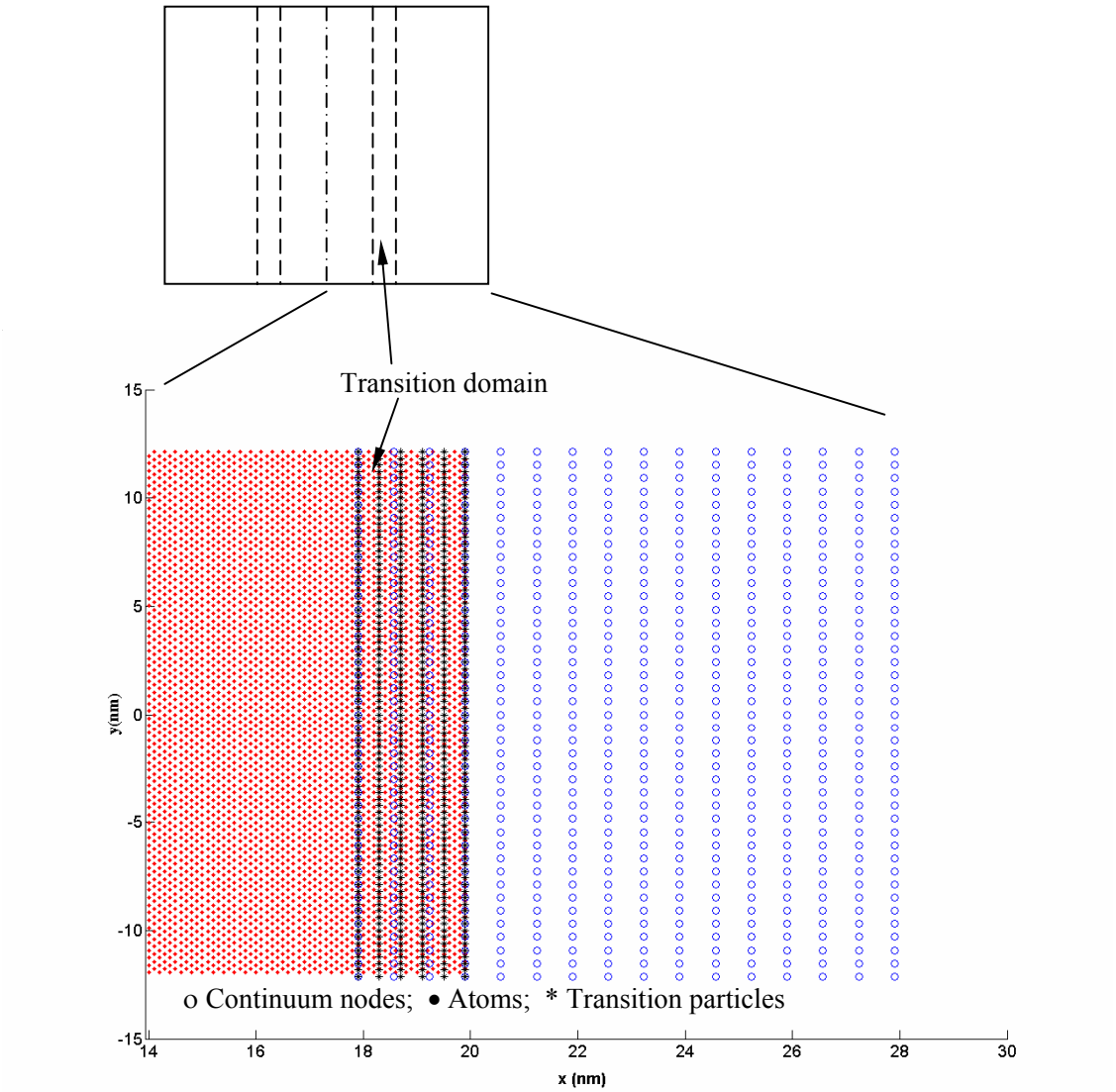

Figure 18. The computational model for 2-D cylinder wave propagation problem

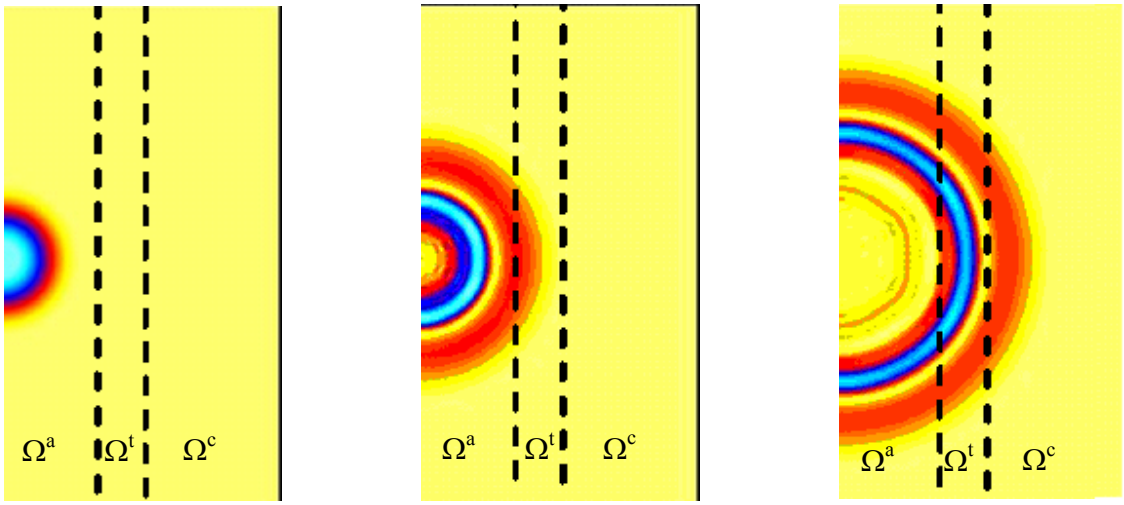

(a) t=0ps (b) t=12ps (b) t=24ps

Figure 19. The circle wave propagation in a 2-D square sheet

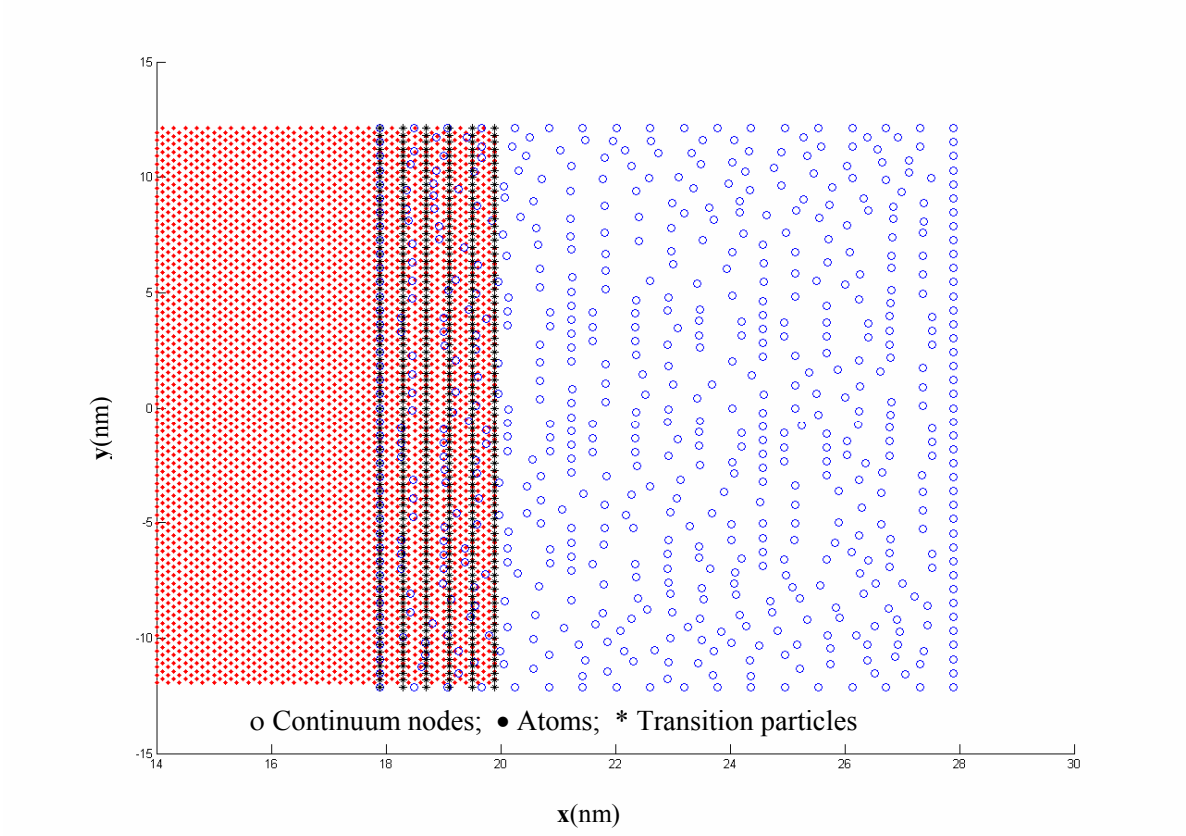

Figure 20. The computational model for 2-D cylinder wave propagation problem using irregularly distributed 636 continuum nodes (the irregular nodes are generated using the MFree 2D® (Liu, 2002) software package)

Reference

Abraham F, Broughton J, Bernstein N and Kaxiras E (1998), Spanning the continuum to quantum length scales in a dynamic simulation of brittle fracture, Europhys. Lett. 44 (1998) 783–787

Atluri SN, Kim HG and Cho JY(1999), A critical assessment of the truly meshless local Petrov-Galerkin (MLPG), and Local Boundary Integral Equation (LBIE) methods. Computational Mechanics, 24,348-372.

Belytschko T, Lu YY and Gu L(1994), Element free Galerkin methods. International Journal for Numerical Methods in Engineering, 37, pp.229-256.

Belytschko T, Liu WK and Moran B (2000), Nonlinear Finite Elements for Continua and Structures, Wiley, New York.

Born M and Huang K(1954), Dynamical theory of crystal lattices. Oxford: Clarendon Press.

Broughton JQ, Abraham FF, Bernstein N and Kaxiras E(1999), Concurrent coupling of length scales: methodology and application. Physical Review B, 60, pp.2391-2403.

Cai W, Koning M, Bulatov V and Yip S(2000), Minimizing boundary reflections in coupled-domain simulations, Physical Review Letter, 85, pp.3213–3216.

Curtin WA and Miller RE(2003), Atomic/continuum coupling in computational materials science. Modelling Simul. Mater. Sci. Eng., **11**, 33–68.

Dupuy LM, Tadmor EB, RE Miller and Phillips R (2005), Finite-Temperature Quasicontinuum: Molercular Dynamic without All the atoms. Physical Review Letter, vol. 95, 060602.

Ericksen JL(1984), Phase transformations and material instabilities in solids. Academic Press: 61-77

Girifalco LA and Lad RA(1956), Energy of cohesion, compressibility and the potential energy functions of the graphite system, J. Chem. Phys. 25, 693–697.

Gehlen PC, Hahn GT and Kanninen MF(1972), Crack extension by bond rupture in a model of bcc iron, Scr. Meter., **6**, 1087–1090.

Gu YT and Liu GR(2001), A meshless local Petrov-Galerkin (MLPG) method for free and forced vibration analyses for solids. Computational Mechanics, 27 (3), 188-198.

E WN and Huang ZY(2001), Matching Conditions in Atomic-Continuum Modeling, Physical Review Letter, **85**, 3213–3216.

Knap J and Ortiz M (2001), An analysis of the quasicontinuum method, Journal of the Mechanics and Physics of Solids, **49**, 1899 – 1923

Kohlhoff S, Gumbsch P and Fischmeister H F(1991), Crack propagation in b.c.c. crystals studied with a combined finite-element and atomic model. Philosophical Magazine A, vol. 64(4), pp. 851-878.

Liang HY and Liu GR(2004), Multiscale Coupling of Meshless Method and Molecular Dynamics. International Conference on computational methods ICCM, 2004, Singapore.

Liu GR (2002), Mesh Free Methods: Moving Beyond the Finite Element Method. CRC press, USA.

Liu GR and Gu YT(2001a), A point interpolation method for two-dimensional solids. Int. J. Muner. Meth. Engng, 50, 937-951.

Liu GR and Gu YT(2001b), A local radial point interpolation method (LR-PIM) for free vibration analyses of 2-D solids. J. of Sound and Vibration, 246(1), 29-46.

Liu GR and Gu YT (2005), An introduction to Meshfree methods and theirs programming. Springer, Berlin.

Onate E, Idelsohn S, Zienkiewicz OZ and Taylor RL(1996), A Finite Point Method in Computational Mechanics. Applications to Convective Transport and Fluid Flow. Int. J. Numer. Methods Engrg., 39, 3839-3867.

Park HS and Liu WK(2004), An introduction and tutorial on multiple-scale analysis in solids. Comput. Methods Appl. Mech. Engrg. 193 (2004) 1733–1772

Park HS, Karpov EG, Klein PA and Liu WK(2005), The Bridging Scale for Two-Dimensional Atomic/Continuum Coupling. Philosophical Magazine, 85 (1): 79-113 JAN 1 2005

Powell MJD (1992), The Theory of Radial Basis Function Approximation in 1990. Advanced in Numerical Analysis, Eds. FW. Light: 303-322.

Rapaport DC(1995): The Art of Molecular Dynamics Simulation. Cambridge University Press.

Rafii-Tabar H, Hua L and Cross M(1998): A multi-scale atomic-continuum modelling of crack propagation in a two-dimensional macroscopic plate. Journal of Physics: Condensed Matter, vol. 10, pp. 2375-2387.

Rudd RE and Broughton JQ(1998), Coarse-grained molecular dynamics and the atomic limit of finite elements. Physical Review B, 58, pp.5893-5896.

Rudd RE and Broughton JQ(2000), Concurrent coupling of length scales in solid state systems. Physica Status Solidi B, 217, pp.251–291.

Sinclair JE(1975), The influence of the interatomic force law and of kinks on the propagation of brittle cracks, Phil. Mag. **31**, 647–671

Shen SP and Atluri(2004), Multiscale simulation based on the meshless local-Petrov-Galerkin (MLPG) method. CMES, 5(3), 235-255.

Tadmor EB, Ortiz M and Phillips R(1996), Quasicontinuum analysis of defects in solids. Philosophical Magazine A, 73, pp.1529–1563.

Xiao SP and Belytschko T(2004), A bridging domain method for coupling continua with molecular dynamics, Computer Methods in Applied Mechanics and Engineering, 193, pp.1645-1669.

Wagner GJ and Liu WK(2003), Coupling of atomic and continuum simulations using a bridging scale decomposition, Journal of Computational Physics, 190, pp.249–274.

Wang JG and Liu GR (2002) A point interpolation meshless method based on radial basis functions. Int. J. Numer. Meth. Eng. 54 (11): 1623-1648.

Wu Z (1992), Hermite-Birkhoff interpolation of scattered data by radial basis functions. Approx. Theory Appl. 8, 1-10.

Zanzotto G(1996), The Cauchy-Born Hypothesis, nolinear elasticity and mechanical twinning in crystals. Acta Cryst. A52: 839-849.

Zhang L and Tanaka (1997), Towards a deeper understanding of friction and wear on the atomic scale - A molecular dynamics analysis. Wear, 211, 44-53.

Zhang L and Tanaka H (1998), Atomic Scale Deformation in Silicon Monocrystals Induced by Two-Body and Three-Body Contact Sliding. Tribology International, 31 (1998) 425-433.

Zhang L and Tanaka H (1999), On the mechanics and physics in the nano-indentation of silicon mono-crystals, JSME International Journal, Series A: Solid Mechanics & Material Engineering. 42, 546-559.

Zienkiewicz OC and Taylor RL (2000), The finite element method (5th edn.). Butterworth Heinemann, Oxford.